Ground-based and additional science support for SMILE

J. A. Carter[1]*, M. Dunlop[2,3,4], C. Forsyth[5], K. Oksavik[6,27], E. Donovon[7], A. Kavanagh[8], S. E. Milan[1], T. Sergienko[9], R. C. Fear[10], D. G. Sibeck[11], M. Connors[12], T. Yeoman[1], X. Tan[3], M. G. G. T. Taylor[13], K. McWilliams[14], J. Gjerloev[15], R. Barnes[15], D. D. Billet[14], G. Chisham[8], A. Dimmock[16], M. P. Freeman[8], D.-S. Han[17], M. D. Hartinger[18], S.-Y. W. Hsieh[15], Z.-J. Hu[19], M. K. James[1], L. Juusola[20], K. Kauristie[20], E. A. Kronberg[21], M. Lester[1], J. Manuel[22], J. Matzka[23], I. McCrea[2], Y. Miyoshi[24], J. Rae[25], L. Ren[26], F. Sigernes[27], E. Spanswick[7], K. Sterne[18], A. Steuwer[28], T. Sun[26], M.-T. Walach[29], B. Walsh[30], C. Wang[26], J. Weygand[31], J. Wild[29], J. Yan[26], J. Zhang[26], and Q.-H. Zhang[32]

[1]Planetary Sciences Group, School of Physics and Astronomy, University of Leicester, University Road, Leicester, LE1 7RH, UK;

[2]Rutherford Appleton Laboratory Space, Science Technology Facilities Council, Oxfordshire, UK;

[3]School of Space and Environment, Beihang University, Beijing 100191, China;

[4]Key Laboratory of Space Environment Monitoring and Information Processing, Ministry of Industry and Information Technology, Beijing 100017, China;

[5]Department of Space and Climate Physics, UCL, Mullard Space Science Laboratory, Holmbury St. Mary, Dorking, Surrey, RH5 6NT, UK;

[6]Birkeland Centre for Space Science, Department of Physics and Technology., University of Bergen, Bergen, Norway;

[7]Department of Physics and Astronomy, University of Calgary, 2500 University Drive, Calgary, Alberta, Canada T2N 1N4;

[8]British Antarctic Survey, Cambridge, UK;

[9]Swedish Institute of Space Physics, Kiruna, Sweden;

[10]West Highfield Campus, University of Southampton, University Road, SO17 1BJ, UK;

[11]Goddard Space Flight Center, NASA, Greenbelt, Maryland, USA;

[12]Athabasca University, Athabasca, Canada;

[13]ESTEC, European Space Agency, Netherlands;

[14]University of Saskatchewan, Canada;

[15]The Johns Hopkins University Applied Physics Laboratory, Laurel, Maryland, USA;

[16]Swedish Institude of Space Physics, Uppsala, SE 75121, Sweden;

[17]Tongji University, Shanghai 200092, China;

[18]Center for Space Plasma Physics, Space Science Institute, 4765 Walnut Street Suite B, Boulder, Colorado, 80301, USA;

[19]Polar Research Institute of China, Shanghai 200136, China;

[20]Finnish Meteorological Institute (FMI), Finland;

[21]University of Munich, Germany;

[22]Canadian Space Agency, Montreal, Canada;

[23]23 GFZ German Research Centre for Geosciences, Potsdam, Germany;

[24]Nagoya University, Institute for Space Earth Environment Research, Center for Integrated Data Science, Nagoya, Aichi, JP 464-8601;

[25]Northumbria University, Newcastle upon Tyne, Tyne and Wear, UK NE1 8ST;

[26]National Space Science Center, Chinese Academy Sciences, Beijing 100190, China;

[27]Arctic Geophysics, University Centre in Svalbard, Longyearbyen, Norway;

[28]EISCAT, Sweden;

[29]Space and Planetary Physics Group, Physics Department, Lancaster University, Lancaster, LA1 4YB, UK;

[30]Boston University, USA;

[31]Earth, Planetary, and Space Sciences, University of California, Los Angeles, USA;

[32]Shandong Provincial Key Laboratory of Optical Astronomy and Solar-Terrestrial Environment, Institute of Space Sciences, Shandong University, Weihai Shandong 264209, China

Key Points:

- Ground-based and other space-based solar-terrestrial facilities will provide cru56 cial multiscale support for the SMILE mission.
- These facilities will bridge the gap between large and ne-scale phenomena.
- The SMILE Ground-based and Additional Science Working Group is developing 59 community tools and data products to aid the scientic exploitation of the mis60 sion.

Abstract: The joint European Space Agency and Chinese Academy of Sciences Solar wind Magnetosphere Ionosphere Link Explorer (SMILE) mission will explore global dynamics of the magnetosphere under varying solar wind and interplanetary magnetic field conditions, and simultaneously monitor the auroral response of the Northern Hemisphere ionosphere. Combining these large-scale responses with medium and fine-scale measurements at a variety of cadences by additional ground-based and space-based instruments will enable a much greater scientific impact beyond the original goals of the SMILE mission. Here, we describe current community efforts to prepare for SMILE, and the benefits and context various experiments that have explicitly expressed support for SMILE can offer. A dedicated group of international scientists representing many different experiment types and geographical locations, the Ground-based and Additional Science Working Group, is facilitating these efforts. Preparations include constructing an online SMILE Data Fusion Facility, the discussion of particular or special modes for experiments such as coherent and incoherent scatter radar, and the consideration of particular observing strategies and spacecraft conjunctions. We anticipate growing interest and community engagement with the SMILE mission, and we welcome novel ideas and insights from the solar-terrestrial community.

Keywords: magnetosphere; ionosphere; magnetosphere--ionosphere coupling; ground-based experimentation; SMILE; conjunctions; missions

Plain Language Summary

The SMILE mission will revolutionise our understanding of large-scale processes in the Earth's dayside magnetosphere by taking X-ray images of the region where the solar wind first impacts the Earth's magnetic field. SMILE will simultaneously image the Northern Hemisphere aurora at ultraviolet wavelengths, and take measurements of the plasma environment in the immediate environs of the spacecraft using two in situ instruments, allowing the chain of cause and effect to be studied in a global context. To maximise the scientific output of SMILE, its measurements must be combined with those from a wide variety of ground-based and space-based experimentation, which provide insights at both medium and fine scales, from both hemispheres, and from the nightside of the Earth's magnetosphere. The Ground-based and Additional Science working group is preparing combined observations using SMILE and other facilities, and is exploring the optimal modes and data products that will best serve the global solar-terrestrial community. The working group is developing tools and software to aid with SMILE science exploitation. We describe these ongoing efforts here, which will naturally increase in breadth and complexity as we approach launch.

1. Introduction

The Solar wind Magnetosphere Ionosphere Link Explorer (SMILE) (Raab et al., 2016; Branduardi–Raymont et al., 2018), is a joint European Space Agency and Chinese Academy of Sciences mission due for launch in 2025. The SMILE Science Working Team consists of several working groups concentrating on various aspects of mission preparation. The Ground-based and Additional Science (GBAS) Working Group is a group of approximately 40 international scientists, including representatives from a range of solar-terrestrial physics observatories and instrument chains around the globe as well as a diverse group of interested collaborators. The remit of GBAS is to coordinate and later implement joint observing campaigns between SMILE and these experiments, whether they be from ground-based or space-based instrumentation.

SMILE will make great strides in understanding large-scale phenomena and discern the modes of the magnetospheric-ionospheric interaction under a variety of interplanetary magnetic field (IMF) and solar wind conditions. However, linking these large-scale phenomena to meso-scale or fine-scale responses in the magnetosphere and ionosphere requires additional observations.

SMILE will carry four science instruments on board: two imagers and two in situ instruments; see the relevant papers in this issue. The Soft X-ray Imager (SXI) will determine the position of the dayside subsolar magnetopause, with the requirement to achieve an accuracy of 0.5 R_E, or approximately 3100 km, under solar wind flux conditions of at least 4.9×10^8 particles $cm^{-2}\,s^{-1}$, with an integration time of 5 minutes (Branduardi-Raymont et al., 2018). The actual integration time to determine the magnetopause position will be variable, and will be dependent on the X-ray emissivity signal to noise at a particular time. The magnetosheath source region X-ray emissivity is dependent on the solar wind heavy ion composition and the exospheric hydrogen density (see for example, Carter (2022) or Sibeck et al. (2018)). The Ultraviolet Imager (UVI), with a field of view trained on the Northern Hemisphere ionosphere, will image the auroral emissions at 100 km scales and 1-minute cadences. The Light Ion Analyser (LIA) is a top-hat analyser that will measure ion spectra in the energy range 50 eV to 20 keV to calculate ion moments at several cadences ranging from 0.25 s to 8 s. The flux-gate Magnetometer (MAG) will measure magnetic field changes ±12,800 nT at 40 Hz with 2 nT resolution.

SMILE UVI will only image the Northern Hemisphere ionosphere, precluding interhemispheric studies. SMILE will also only make limited in situ measurements on the nightside of Earth, due to the orientation of its highly elliptical polar orbit. ESA has recently recognised the need to combine space and ground-based measurements, when it said in a recent report regarding the Swarm (Friis-Christensen et al., 2008) mission "A holistic view of the Earth−Sun system can only be provided by a multi-mission interdisciplinary approach to science where Earth Observation satellites, data and science results are combined with ground-based facilities and also other ESA missions both ongoing …. And in the near future (e.g., SMILE, …)", see Section 7. The need to fill the knowledge gap between large-scale (e.g. SMILE) and fine-scale features (e.g. in situ particle measurements), is well recognised in the solar terrestrial community (see for example an overview discussion of the topic by Carter et al. (2022)). SMILE will obtain the broadest science by eliciting support of other experiments at a range of spatial and temporal scales and in both hemispheres to provide context and a holistic system-wide view of any phenomena under study.

Built up over decades, there is a wealth of ground and space-based experimentation that can complement SMILE's global observations and fill in the details of related fine- and mesoscale structures thought to be essential components of the overall solar-terrestrial interaction. By working together, the reach and scope of the SMILE mission will be extended well beyond its original goals, and will achieve much more than any of the experiments in isolation. These experimental facilities provide inter-hemispheric, global, regional, and local measurements at multiple spatial scales and cadences. We build on experience and good-practice obtained by the community during collaborations between space and ground-based missions, such as the European CLuster AssimilaTion project (ECLAT, (Milan et al., 2013), see Section 7) or as reviewed in Fear (2022) or Amm et al. (2005). Best practice indicates

that early inclusion of the ground-based community before launch leads to the widest range of timely scientific return.

2. Overview of Currently Collaborating Resources

The wide breadth of experiments and space-missions currently collaborating in the GBAS WG represents many different solar-terrestrial experiments. Below we describe the resources available for collaboration through participants that sit on the GBAS Working Group at the time of writing, but we recognise that there are many further possible avenues for collaboration and welcome wider participation in the working group. The user base for SMILE data is likely to increase during the operational mission and also after decommissioning when exploitation of the SMILE archive will be encouraged. We envisage a growing community of scientists willing to actively participate in the SMILE mission as we move towards and post launch, and we welcome new collaborations, and data processing and product ideas.

SMILE will be initially commissioned for a 3-year mission, but it has a maximum mission lifetime of 7 years post launch. On the current schedule, the upper limit of SMILE's operational phase will come to an end in the first quarter 2032. By this time, multi-point missions such as NASA's Geospace Dynamics Constellation (Pfaff, 2020) and Tandem Reconnection and Cusp Electrodynamics Reconnaissance Satellites (TRACERS) will be operational. The Lunar Environment heliospheric X-ray Imager (LEXI, B. Walsh et al. (2021)), using similar technology to the SXI instrument, will have completed its mission. We look forward to collaborating in the future. We consider several combined mission tools, such as with the Electrojet Zeeman Imaging Explorer (EZIE) and Swarm missions, in Section 5.

In Figure 1 we show a schematic of the ground-based facilities and experiments that have, to date, expressed support of SMILE and have representation within the GBAS WG, and these are tabu-
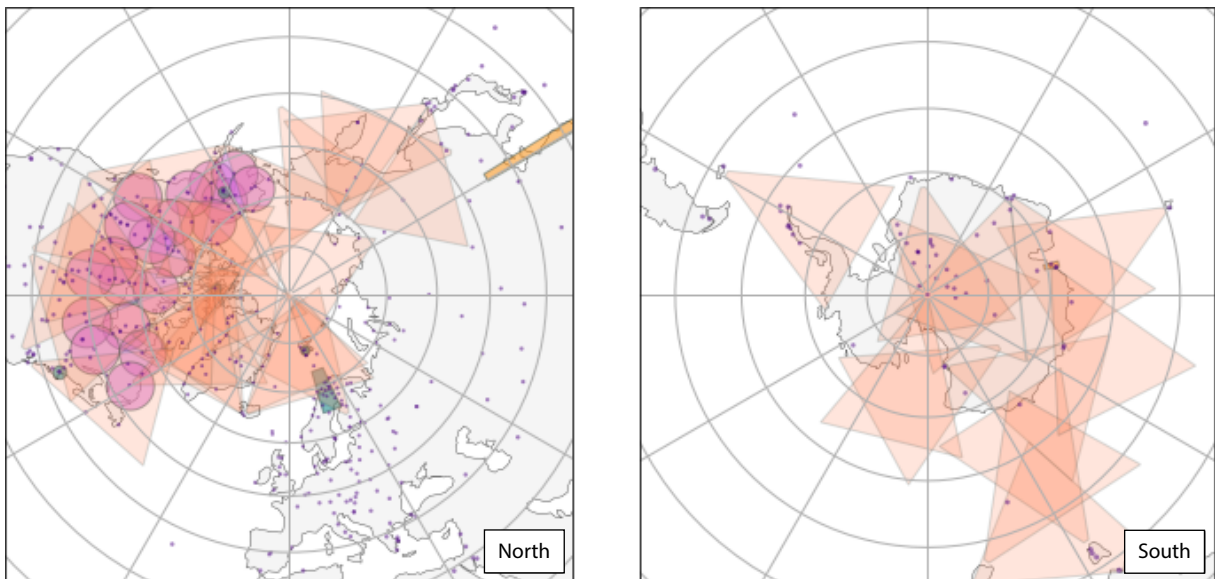
Figure 1. Ground-based facilities that have explicitly expressed support for the SMILE mission at the global and regional scale (local measurements are not shown). Left and right panels show projections in the Northern and Southern hemispheres respectively. Facilities are shown as fields of view or locations for point measurements (see main text): SuperDARN (coral-colored fans), EISCAT Svalbard and EISCAT 3D and various ISR radar (teal), SMILE ASI (pink circles), Meridian (orange), SuperMAG (purple dots).

Table 1. Ground-based facilities, consortia, or collaborations that have explicitly expressed support for the SMILE mission to date.[a]

Facility	Experiment type	Location	Coverage	Major data product	Temporal resolution	Spatial resolution
SuperDARN	Coherent scatter radar	Multiple sites	Global	Ionospheric convection maps	1-min	45 km (standard), 15 km (other modes)
SuperMAG	Magnetometers	Multiple sites	Global	Magnetic field perturbations	1 min or 1 s	
SMILE ASI	Imagers	North America	Regional	Images	3 s	few km
CMP	Multiple	China, Amer3 s Antarctica	Regional	Multiple	Multiple	Multiple
EISCAT & EISCAT 3D	Incoherent scatter radar	Scandinavia	Regional	Ionospheric electron densities, ion flow velocities, ion & electron temperatures	Multiple	Multiple
AUTUMN	Magnetometers	Canada	Regional	Magnetic field perturbations	0.5 s	
KHO	Multiple	Svalbard	Local	Images & emission spectra	μs to hours	100 m
Watec, MIRACLE, IMAGE, ALIS4D	Multiple	Fennoscandia	Local	Images & Magnetic field perturbations	μs to s	100 m

[a]Listed by experiment type, location, coverage, main product, and temporal and spatial resolution (where applicable) of the main data product. Some facilities, such as SuperDARN, have multiple products, modes and resolutions possible. Only the major data products are listed here. The only incoherent scatter radar (ISR) listed here, for brevity, is EISCAT. Other ISR are described in the main text.

lated in Table 1. We briefly describe these facilities below, and separate these facilities into broad categories of those with global, regional, or geographically-constrained spatial coverage. We only show the largest global and regional-scale facilities in this figure given the scale of the images.

2.1 Global, All-year Coverage

Global, all-year coverage of ground-based measurements is provided by networks of coherent scatter radars (the Super Dual Auroral Radar Network, SuperDARN) and several ground magnetometer networks including those that are part of the global SuperMAG collaboration.

SuperDARN is a network of coherent scatter radars that operate in both hemispheres (Chisham et al., 2007). However there is considerably more coverage in the northern hemisphere due to its larger landmass, accessibility, and infrastructure. SuperDARN radars transmit at high frequency (approximately 8 to 20 MHz) and this signal is backscattered by field-aligned decametre irregularities in the F-region ionosphere. SuperDARN measures line-of-sight velocity, backscattered power, and the width of the Doppler-shifted power spectrum of the returned signal. Data processing steps involve finding a description for the distribution of electrostatic potential in the ionosphere that best fits the line-of-sight velocity measurements, in the form of a spherical harmonic function (Chisham et al., 2007). Velocity measurements are obtained at 45 km spatial resolution and ionospheric convection maps produced every minute, in standard operational modes. The SuperDARN network is managed as a consortium of member institutions, and each institution is responsible for obtaining their own funding via national funding agencies. As such, new radars have

become operational and have joined the network from the commencement of the SuperDARN project consortium in 1993, following the build of the first individual radar at Goose Bay in 1983, including polar, high-latitude and mid-latitude stations. Data are made available via member institutes and data mirrors, see Section 7. Additional radar data from coherent radar stations in the northern Russian sector, outside of SuperDARN, are available on request, see Section 7.

Recent localised adaptations to several SuperDARN radar systems have been made by installing the Borealis (McWilliams et al., 2023) digital radar systems developed at the University of Saskatchewan. The new system uses Universal Software Radio Peripheral (USRP) technology and associated control software to meet the hardware requirements of a new ionospheric coherent scatter radar system. The use of the USRPs eliminates the requirement for analogue beam forming (where the signals from all antenna systems are combined together through a fixed phasing matrix before being passed to a single receiver), but instead digitally samples all individual antennas separately before digitally combining the signals. These USRPs also provide many opportunities to expand the capabilities of the SuperDARN radars to accommodate experiments of higher spatial and temporal resolution and greater complexity. At the same time, the software makes experiments easier to write and interpret by researchers. Incorporating this system into the network will allow us to produce new radar modes for ground-space conjunction campaign operations.

There are magnetometer networks operated by a wide range of organisations around the world that are of use to the SMILE Mission. These include magnetometers that are part of the Super-

MAG collaboration, which generates higher level data products used to infer the global electric current system (Gjerloev, 2012), produce various indices representing different current system components, and identify transient (1−20 min) events in the solar wind-magnetosphere interaction. Magnetic indices are available through many channels, including the SuperMAG website and also the commonly used and freely available OMNI (King and Papitashvili, 2005) data set (see Section 7). As well as the traditional three-hourly Kp index (Matzka et al., 2021), the Kp-like Hpo indices (half-hourly Hp30 and hourly Hp60) recently became available and have been shown to reproduce the short-term (< 3 hours) geomagnetic activity related to substorms (Yamazaki et al., 2022). Ground magnetometers can be used to infer ionospheric convection patterns and identify transient (1−20 min) events in the solar wind-magnetosphere interaction.

2.2 Regional Coverage

Regional coverage is provided by ground-based auroral imagers, incoherent scatter radar, and localised magnetometer chains.

NASA's Time History of Events and Macroscale Interactions during Sustorms (THEMIS) is a five satellite mission launched in 2007 with the primary scientific objective of determining the mechanism of substorm onset (Angelopoulos, 2008). The mission science warranted knowledge of the onset meridian (e.g., longitude) for substorm events. In order to address this, the mission included a continent-wide network of All-Sky Imagers that would capture mosaics of the aurora across Alaska and Canada, and into Greenland. The 21 imager THEMIS-ASI network was deployed during 2005−2007 and has since been capturing panchromatic (white light) images of the night sky with several kilometre spatial resolution and 3 second cadence (Donovan et al., 2006a; Mende et al., 2008). The THEMIS-ASI network has given us a new window into mesoscale geospace processes and their importance to space weather at the system level (e.g. Lyons et al. (2013)). For SMILE, the key point is that a network such as THEMIS-ASI, which is by far

the most geographically extensive of its type globally, extends coverage of the space-time dynamics of the aurora beyond the one minute, 60 second global UV images anticipated from SMILE-UVI.

The THEMIS-ASIs have been operating in harsh arctic conditions for 18 years. The support electronics and CCD detectors are rapidly approaching end-of-life. In support of the SMILE mission, and because THEMIS-ASI is a facility that is widely depended upon by the global geospace research community, the Canadian Space Agency has approved the replacement of the network with a new set of imagers and support electronics. This new network will be called SMILE-ASI and will consist of at least 19 full colour (or RGB) ASIs. As can be seen in Figure 2, the SMILE network will have slightly less east−west coverage, and slightly greater north−south coverage than its predecessor, a deployment which is believed will better suit the SMILE mission science. The new imagers will begin being deployed in the summer of 2023, with the complete replacement of THEMIS-ASI (those imagers will be decommissioned as the SMILE imagers are commissioned) by summer 2025 at the latest. The new ASIs will provide a panchromatic THEMIS-equivalent data stream, estimated oxygen green line intensity images, and the full RGB images. The replacement of THEMIS-ASI is an indication of support for SMILE, and a first step towards the establishment of a 'permanent' continental scale All-Sky Imaging facility in North America that will extend through further upcoming missions such as NASA's Geospace Dynamics Constellation, and other possible even longer-term missions such as Magnetospheric Constellation.

Regional measurements with potentially, but not necessarily continuous, year-round coverage are also provided by a variety of incoherent scatter radar. These radars primarily operate at high-latitude northern locations (see Figure 1 that shows the high-latitude ISR only, see text below for more details). They measure the electron density, electron and ion temperatures, and line-of-sight

Figure 2. Map of the current THEMIS ASI (dotted circles) and the future SMILE (thick, multiicoloured circles) ASI networks across North America, showing the field of view of the cameras. The SMILE ASI network extends to higher and lower latitudes, whereas the THEMIS ASI coverage is wider in the east−west direction.

ion drift velocity at high cadence. Radar measurements are typically made in the altitude range from 80 to 1000 km. ISR can be used to determine pulses in the magnetopause reconnection rate (Wild et al., 2001; Lockwood et al., 2005), and flow shears and ion up-flow events associated with poleward moving auroral forms (Oksavik et al., 2004; Moen et al., 2004), the traversal of electron density patches in the polar cap (Carlson et al., 2006; Oksavik et al., 2010).

The European Incoherent Scatter Scientific Association (EISCAT) operates radars in Svalbard and northern Scandinavia. Investments and operational costs are shared between the EISCAT Associates in China, Japan, UK, Norway, Finland and Sweden, with smaller contributions from institutes in Germany, South Korea, Ukraine and the USA. American radars are funded by the National Science Foundation (NSF) and operated by SRI International (PFISR, RISR-N (Bahcivan et al., 2010)) and the MIT Haystack Observatory (Millstone). The RISR-C radar is operated by the University of Calgary (Gillies et al., 2016). RISR-N and RISR-C are in the central polar cap, whilst the EISCAT Svalbard Radar (ESR) observes the ionospheric footprint of the cusp and the poleward edge of the nighttime auroral oval. PFISR and the mainland EISCAT radars observe the auroral oval, and additional coverage of the mid-latitude sub-auroral zone is offered by the Millstone Hill radar. ISR observations also extend from the mid-latitude to the equatorial region.

EISCAT is constructing a major upgrade to its radar facility on the Scandinavian mainland, replacing the existing radars. EISCAT_3D is a high-power, phased array radar capable of three-dimensional imaging of the ionosphere (McCrea et al., 2015). Digital beam forming and rapid switching will allow effectively simultaneous beams in multiple directions, enabling multi-scale measurements, including interferometry to sub-beam scales. The initial system will have a transmit power of 3 MW and three receiver sites that will combine to produce a vector of the ion-drift, distributed in the volume of view. Due to the power of the system a high time resolution is expected, but absolute numbers will be dictated by the state of the magnetosphere–ionosphere system; sub-second observations are anticipated with an altitude resolution of a few hundred metres, depending on selected pulse coding. The overall field of view will depend on the experiment being operated at a given time, and the rapid switching means that multiple experiments can operate simultaneously. The lowest elevation of the beams is 30 degrees, which would give a horizontal, circular field of view at 250 km altitude with a radius of 430 km and a potential coverage of over 7 degrees of latitude. Construction of phase 1 is currently underway, with initial operations aiming to begin later in 2023. Additional construction phases may increase the overall transmit power to 10 MW and add more receiver sites to boost the density of volumetric measurements (if additional funding becomes available).

The Chinese Meridian Project (CMP, Wang C, 2010; Wang C et al. 2020, 2022), a comprehensive ground-based monitoring network of the space environment, includes 31 stations with nearly 300 instruments mainly deployed along geographic 100°E and 120°E longitudes and the 30°N and 40°N latitudes. The fundamental strategy of CMP is to use a combination of geomagnetic, radio and optical instruments to monitor Earth's space environment over China. Instruments include, amongst others, ground magne-

tometers of various types, imaging devices such as Fabry–Perot interferometers and auroral spectrometers, coherent scatter and ISR, and ionosondes. Its first phase was put into operation in 2012, and the second phase will be completed by the end of 2023.

In the Earth's ionosphere and upper atmosphere, space environment disturbances can propagate from high latitudes to middle and low latitudes, sometimes along the Great Meridian circles. To take advantage of this feature, CMP deploys a network with a series of powerful and innovative equipment covering from high to low latitudes. For example, in polar regions, the Yellow River and Longyearbyen stations are deployed in the Arctic, and the Great Wall and Zhongshan stations are deployed in the Antarctic. In the northern region of China, which is a pathway for disturbances propagating from high-latitude regions towards middle and low-latitude regions, a six-frequency HF radar system, operating as part of the SuperDARN network, provides 2D observations of ionosphere plasma drifts and irregularities. On Hainan Island, which is closest to the equatorial anomaly, the Sanya three-station ISR will provide three-dimensional measurements of the low-latitude ionosphere.

In addition, CMP is building a series of advanced solar interplanetary monitoring equipment to monitor the whole space weather chain from the Sun to Earth, which includes two solar radio telescope arrays to observe solar activities and a three-station interplanetary scintillation telescope system for interplanetary observations. Coordinated operation of CMP with the SMILE mission will make it possible to observe the propagation of space weather events from the Sun to Earth, detect space weather effects in polar regions, and finally track their propagation towards middle and low latitudes along the meridian circles, deepening our understanding of solar wind/magnetosphere/ionosphere coupling processes.

The recently expanded Athabasca University THEMIS UCLA Magnetometer Network (AUTUMN) East–West magnetometer chains (Connors et al., 2016) will support SMILE by detecting magnetic pertubations in both the far east and far west of Canada. The ground-stations in this chain are located at the standard magnetic footprints of the Geostationary Operational Environmental Satellite (GOES) East and West geostationary spacecraft along approximately two meridian lines spanning the auroral zones. The eastern Canadian chain complements the Meridian network chain in China in the eastern hemisphere, and is a conjugate to stations in Antarctica. The GOES space weather monitor capabilities working together with the AUTUMN chain are providing important measurements in understanding geomagnetically-induced currents (GICs) in a geographical area that is important for energy generation, yet vulnerable due to the geological surroundings. SMILE will provide the global context for understanding space weather impacts such as geomagnetically-induced currents.

Measurements from the above networks, as well as magnetometers in Greenland operated by the Technical University of Denmark can be combined with several existing networks of magnetometers in Antarctica to produce 1D and 2D inter-hemispheric comparisons of wave activity and mesoscale current

systems in the auroral zone, cusp, and polar cap (Clauer et al., 2014; Shi X et al., 2020; Xu Z et al., 2020; Engebretson et al., 2022).

2.3 Localised Coverage

Facilities at a local scale are also represented in the GBAS Working Group. These facilities can provide fine-scale, high-cadence measurements in restricted geographical areas.

In winter, auroral emissions can also be observed from the ground with high temporal and spatial resolution, when the Sun is at least 10–12° below the horizon. New-moon periods are best, as moonlight may compromise optical data. The local weather must cooperate, so the sky is not entirely covered by clouds. The location and size of the auroral oval is influenced by geomagnetic activity. The offset between the geographic and magnetic poles puts additional constraints on when and where the aurora can be observed.

In the Northern Hemisphere, from the ground, the cusp aurora can only be observed from the archipelago of Svalbard, from 06:00 to 12:00 UT, and between approximately November 20 and January 20. In this period the entire Northern Hemisphere auroral oval is in darkness, as shown in the left panel of Figure 3. In 2008 a new auroral observatory was opened; the Kjell Henriksen Observatory (KHO). KHO is located next to the EISCAT Svalbard Radar, in Longyearbyen. KHO is the largest auroral observatory in the world, with nearly 40 instruments from 18 institutions in 11 countries. The instruments track the motion, spatial extent, and color spectrum of the aurora on temporal scales ranging from milliseconds to hours, and spatial scales ranging from hundreds of meters to hundreds of kilometres. An example of a simulation of a composite colour image from a very intense cusp aurora is shown in the right panel of Figure 3. The dayside cusp aurora over Svalbard has been characterised as a function of interplanetary magnetic field using this observatory (Sandholt et al., 1998). In Svalbard, there are also a handful of additional auroral imagers operated by the Chinese Yellow River Station (Ny-Ålesund) and the University of Oslo (Ny-Ålesund and Hornsund). Data from Svalbard are approximately magnetically conjugate with the Chinese Zhongshan Station in Antarctica, which allows for simultaneous observing of the northern and southern hemisphere cusps in winter.

Also in the Finnish–Scandinavian sector, the Magnetometers Ionospheric Radars All-sky Cameras Large Experiment (MIRACLE) is a geophysical instrument network operated as an international collaboration under the leadership of the Finnish Meteorological Institute (FMI). The International Monitor for Auroral Geomagnetic Effects (IMAGE) magnetometer network is the oldest part of MIRACLE. IMAGE consists of 56 magnetometer stations maintained by 10 institutes from Finland, Germany, Norway, Poland, Russia, Sweden, Denmark, and Iceland. The IMAGE stations are located at geographic latitudes from approximately 51° to 79° and provide data covering the whole auroral region from the main ionospheric trough to the polar cap. Those IMAGE locations forming a meridional chain are especially useful for studying the equivalent ionospheric currents. The IMAGE observations are the base for algorithms developed in FMI for deducing the 1D and 2D ionospheric currents that are successfully used to study the ionosphere–magnetosphere processes and are potentially important for the SMILE mission (Amm and Viljanen, 1999; Amm et al., 2013). The Auroral Large Image System 4D (ALIS4D) multi-wavelength auroral imager network is operated by the Swedish Institute of Space Physics. ALIS4D consist of six unmanned remote-controlled auroral imagers in Northern Sweden. These imagers have extremely high time resolution of greater than 25 images per second, and good spatial resolution on the order of 100 m. The overlapping fields of view at an altitude of approximately 80 km allows for tomographic reconstructions of 3D auroral structures (Tanaka et al., 2011). Various Japanese-run auroral imagers, such as the Watec network, operate from this region (Shiokawa et al., 2017; Ogawa et al., 2020). Coordinated ALIS4D, MIRACLE, and Watec measurements, especially considered if in collaboration with SMILE-ASI, will allow coverage of auroral structures over large swathes of local time at multiple temporal and spatial scales.

Additional southern hemisphere auroral monitoring may be provided by optical measurements obtained at South Pole
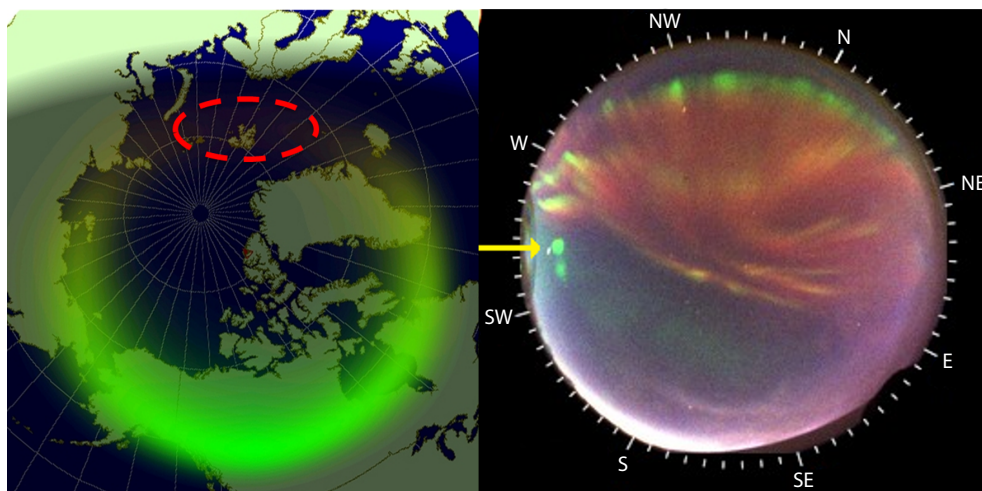
Figure 3. (Left panel) Between 06:00–12:00 UT Svalbard is under the dayside cusp aurora (indicated by a dashed red ellipse), and from November 20 to January 20 the entire Northern Hemisphere auroral oval in darkness; (Right panel) a composite colour image of how a very intense cusp aurora may look like from the ground through an intensified all-sky imager.

stations. These observations can provide a conjugate view from the southern hemisphere of the phenomena that will be tracked in the northern hemisphere by the UVI. Networks of magnetometers stretching from Greenland to Svalbard have conjugacy with stations in the Southern Hemisphere, allowing for interhemispheric studies of current systems, contemporaneous with the in situ measurements of SMILE, and in the context of the influence of dayside driving as monitored by the SMILE SXI and UVI imagers.

Auroral precipitation, particularly of higher energy (tens of keV) electrons, significantly affects ionization in the D-region of the ionosphere, where electron–neutral collisions cause significant absorption of radio waves in the HF (tens of MHz) band. When the power of an HF signal in the absence of this ionospheric attenuation is known, its relative attenuation can be used as a means for remotely sensing such high-energy electron precipitation. Relative Ionospheric Opacity Meters (Riometers) are ground-based radio receivers that passively observe HF band Galactic radio noise, a known signal (Little and Leinbach, 1959). A given riometer and a given geographic position will have a characteristic quiet day curve, deviations from which we call absorption. Riometers have a significant advantage over optical auroral observations in that the quality of the signal in terms of identifying such high-energy precipitation is independent of cloud cover and daylight (e.g. Kavanagh et al. (2009)); however, that information is relevant only to higher energy precipitation, and the spatial resolution afforded by riometers is in general quite poor.

The precipitation that causes most riometer absorption is comprised of central plasma sheet (CPS) electrons that have been energised and nudged into the loss cone by wave-particle interactions. Provided these electrons are strongly affected by pitch angle scattering, the time series of riometer absorption is an excellent proxy for the time series of integrated flux of 10 s to ~100 keV electrons on the flux tube that is magnetically conjugate to the riometer (Baker et al., 1981). This fact was used to identify the signature of dispersionless injections, related to the beginning of substorm expansion phase onset, in time series of riometer data (Hargreaves et al., 1975; Spanswick et al., 2007). With this, it is now clear that networks of imaging riometers, for example the Transition Region Explorer (TREx) that places a set of riometers across a large region of Canada, can be used to create 2D time evolving maps of the changing high-energy electron population in the near-Earth CPS around substorm onset.

2.4 Currently Collaborating Space-Based Experiments

The GBAS Working Group includes members that represent several ongoing currently orbiting or planned spacecraft investigating near-Earth space. Data are, or will be, freely available from portals such as CDAweb (see Section 7).

The in situ measurements of the four Cluster spacecraft (Escoubet et al., 2001) have been combined with ground-based measurements throughout the mission, and this association has been embedded within the Cluster consortium since before launch in 2000 (Fear, 2022). There is a possible brief window of joint Cluster-SMILE operations if the Cluster mission is extended beyond its current mission end up to a maximum of August 2026, and SMILE remains on its current schedule. Along with other magnetospheric

spacecraft arrays, such as THEMIS (including the ASI, as described in Section 2.1) and the Magnetospheric Multiscale (MMS), there is therefore a long history of combining multi-point measurements covering different regions of the magnetosphere.

Since 2013, ESA's Swarm mission, which consists of 3 spacecraft flown in formation, has also provided multi-point measurements from the upper ionosphere, in its LEO, near polar orbit at altitudes of 460 km and 530 km. Swarm is able to measure field-aligned currents (FACs) at high accuracy through the highly calibrated, high cadence (normal mode 50 Hz) magnetic field measurements. Swarm operations routinely provide fine-scale, dual and single spacecraft estimates as standard L2 data products, with a polar pass every 90 mins, as well as the capability to apply additional analysis techniques to access the electric current density, derived from the Curlometer method (Dunlop et al., 2021), which was originally developed for the Cluster array. Early work on Swarm during its close, 3-satellite constellations showed that similar profiles of FACs at Cluster and Swarm could be seen during conjunctions (Dunlop et al., 2015), implying that FACs at Swarm are echoed at Cluster on the same field-lines and thus that coherent structures exist at vastly different altitudes. In addition, Swarm routinely flies with two satellites (A–C) side by side, allowing current sheet alignments to be estimated from FAC cross-correlations (Yang JY et al., 2018).

These Swarm fine-scale measurements can be used in the context of larger scale, cruder measurements from the Active Magnetosphere and Planetary Electrodynamics Response Experiment (AMPERE, Anderson et al., 2000; Waters et al., 2020), which provide maps of both northern and southern hemisphere FACs from 700–800 km altitudes, at 2 min cadence on a 1 deg magnetic-latitude, 1 h magnetic local time (MLT) grid. For the large scale, and large amplitude currents it can be shown that scaled FACs measured by both Cluster and Swarm are consistent with the AMPERE model currents (Dunlop and Lühr, 2020). Swarm is currently also complemented by additional satellites operating 'platform magnetometers' at similar altitudes to Swarm (CSES, Cryosat2, Grace-FO), and these, together with the Canadian Cassiope mission provide an extended, coordinated LEO data set. Swarm has planned operations through 2030. NanoMagSat, a candidate three satellite scout mission, is currently under review for launch post-2025. It is designed to complement Swarm operations with two, 12-U nanosatellites aimed at (approximately) 60° inclination and one polar, circular, 500 km altitude orbits.

The spatial extent, location, and magnitudes of both the region 1 and region 2 FAC systems have been shown to respond in a manner consistent with the expanding/contracting polar cap model of the Dungey Cycle (Coxon et al., 2014; Milan et al., 2017, and references therein). These missions together represent a huge resource of clustered, multi-point (and multi-scale) measurements which can be coordinated with the SMILE data set and in the context of its estimates of dayside reconnection.

EZIE (Yee et al., 2022) is the first mission to apply Zeeman-splitting techniques to remotely sense the magnetic signatures of the ionospheric electrojets and provide multipoint vector magnetic field measurements proximate to their source current. This will

reveal both the spatial structure and the temporal evolution of the auroral electrojets. The EZIE mission comprises 3 6U-class satellites that will fly in a loose pearls-on-a-string configuration in a near-circular, Sun-synchronous, low-Earth orbit of around 500 km altitude about the noon-midnight plane, and are due for launch no earlier than mid 2024. Each EZIE satellite will image the magnetic fingerprint of the electrical current simultaneously at different locations using a push-broom configuration made up of 4 beams in the cross-track direction, probing distances between 150 and 500 km at 3 s integration. EZIE's Microwave Electrojet Magnetogram instruments use the Zeeman effect to infer magnetic fields at 80 km altitude. This technique has been extensively applied to study the Sun's magnetic field, whereas EZIE now applies it to the Earth. EZIE's science goals are to investigate the structure and evolution of the auroral electrojet, in relation to the substorm current wedge (SCW) and its dynamics (Kepko et al., 2015; Gjerloev and Hoffman, 2014). The baseline mission duration is 18 months, which on current schedules will run concurrently with SMILE.

The Defense Meteorological Satellite Programme (DMSP) spacecraft, of which two are currently in operation, take both in situ measurements of precipitating electrons and ions, as well as images of auroral emissions at five wavebands from the Special Sensor Ultraviolet Spectrographic Imager (SSUSI) (Paxton and Anderson, 1992; Paxton and Zhang, 2016). The satellite orbit at about 850 km at fixed local times, so that swaths of high-latitude aurora are detected during each polar cap pass of the spacecraft approximately once every 1.5 h. Native pixels are binned into super pixels of size 25 km by 25 km. The future of these spacecraft is somewhat uncertain, but if still operational from the SMILE launch onwards, the SSUSI multi-band imagers would provide useful constraints on the energy of precipitating particles in more localised regions, and would used in context of the complete northern hemisphere polar cap single-band image to be made by SMILE UVI.

The NASA's TRACERS mission, due for launch in 2024, consists of two identically instrumented spacecraft making observations in the cusp in 500 km altitude, sun-synchronous circular orbits with the spacecraft separated by 10 s to 120 s. Instrumentation willl provide electric and magnetic field measurements and ion and electron detectors. The TRACERS two-year mission will provide over 6000 northern cusp crossings, and is partnering with the Hankasalmi Auroral Imaging Radar System (HAIRS) project within the SuperDARN consortium, see Section 2.1. This represents an opportunity of making conjugate ground-space cusp measurements for the longitude of a given SuperDARN radar once every day of joint operations, an opportunity in stark contrast with the rare chance conjunctions typically used between single LEO spacecraft or elliptically-orbiting spacecraft, which spend very little time on cusp field lines, which have been possible to date. TRACERS will cross the cusp in 30−120 s at a velocity of 7.5 km s^{-1}, faster than the cusp convection velocity. This is required to unambiguously distinguish between temporal and spatial structures. Spatial separation of the TRACERS spacecraft corresponding to less than 2 minutes in cusp crossings will allow specific features in the spacecraft data to be correlated, with much higher precision

than previous chance encounters where separations were typically tens of minutes. During this multitude of space-ground conjunctions, TRACERS will measure cusp particles and fields, whilst SuperDARN will provide purpose-designed high resolution observations of the cusp region, remote sensing the spatial and temporal structuring of the electrodynamics. The large database of TRACERS cusp crossings will allow the full separation of phenomena by upstream conditions such as interplanetary clock angle and solar wind dynamic pressure.

2.5 Support for Main SMILE Mission Goals

SMILE has three main science objectives. These are 1) *What are the fundamental modes of the dayside solar wind/magnetosphere interaction?* 2) *What defines the substorm cycle?* and 3) *How do Coronal Mass Ejection driven storms arise and what is their relation to substorms?* The ground-based community will make significant contributions to these questions, by making specific coordinated observations that will complement those provided by SMILE. We provide some examples below, focusing on the contribution of supporting ground-based experiments.

For science objective 1, ionospheric plasma flows (SuperDARN) and ionospheric convection pattern changes can be tracked (SuperMAG, AUTUMN East and West etc.) after initiation of reconnection at the dayside (SMILE-SXI), along with the detection of smaller-scale transient phenomena such as travelling convection vortices. These phenomena can be compared to the evolution of the movement of the dayside magnetopause following magnetic reconnection, for example whether the ionospheric signatures of reconnection match or contradict the either steady or sporadic motion of the magnetopause. Cusp aurora, Joule heating, ion upflows, and the tracking of newly opened magnetic flux tubes can be tracked from regional or localised measurements (Svalbard, Meridian, and Antarctic experiments, ISRs).

For science objective 2, the substorm will be tracked through triggers on the dayside, and later on the nightside by ground-based experiments, following the monitoring of the prevailing dayside conditions that provoke or prime the system for substorm initiation by SMILE. Nightside auroral imagers (SMILE-ASI, Scandinavian imagers, Meridian chain) will provide meso- and fine-scale images of the substorm auroral bulge and breakup, and be used to confirm the changing open-closed field-line boundary and implied change in open magnetic flux enclosed by the polar cap, as obtained by SMILE-UVI. Two-dimensional spatial–temporal evolution of the dispersionless injection following the substorm will be monitored by individual or networks of riometers (e.g. TREx). The cusp spot aurora will be tracked as it moves either equatorward or poleward during the cycle. The cusp spot can be observed regardless of time of year, as either stations in the northern or southern hemisphere can be used (e.g. Svalbard, Meridian, Antarctica). Substorm commencement via mechanisms such as auroral streamers will be obtained from radar (SuperDARN, ISR). The frequency and conditions for substorms can be tested using this holistic approach.

For science objective 3, extremes in geomagnetic indices will be obtained (SuperMAG, AUTUMN-X East and West) during CME-driven storms. Auroral imagers will track CME-driven storms in a similar manner to science objective 2. Changes and differences

between substorm and geomagnetic storms will be determined by radar (SuperDARN, ISRs), and the influence of the ring current in inhibiting storm and substorm onset can be tested (e.g. Cluster, geomagnetic indices).

3. Highlighted Science Questions with a Strong GBAS Contribution

Here, we present a set of four example science questions within the wider global aims of the SMILE mission, representing a small subset of open questions within the field. These questions will only be answerable given ground or other space-based support for SMILE. These are shown in the schematic in Figure 4.

### 3.1 Question 1: What are the Key Physical Processes at Substorm Onset?

A primary science goal of SMILE is to investigate the substorm cycle, from solar wind coupling and magnetospheric reconfiguration on the dayside, as observed by SXI, to the large-scale ionospheric response seen in the main auroral oval boundary by UVI. In situ measurements by SMILE in the high-latitude magnetosheath, using field-line tracing techniques, may also give some indication as to the variation in conditions within this boundary that may impede or enhance this coupling. However, while this coupled global view will provide new context on the large-scale variations in the magnetosphere prior and during substorm activity, some key elements, such as substorm onset itself, require high time and high spatial resolution of the aurora, ionospheric flows and conductivities and coupled magnetospheric measurements of the relevant source regions.

The mechanism or mechanisms that control the start of a substorm continue to be hotly debated in the community. Figure 5 illustrates two of these mechanisms. Observations from all-sky imagers over the past decades have shown the apparently obiquitous occurrence and growth of spatially period auroral forms, now called "auroral beads", on the substorm onset arc (Donovan et al., 2006b; Forsyth et al., 2020, and references therein), and Figure 5 left-hand panel. These beads have been shown to grow exponentially across a range of scales at almost all examined substorm onsets (Nishimura et al., 2016; Kalmoni et al., 2017). Their exponential growth is indicative of these beads being the "fingerprint" of a plasma instability in the magnetotail (Liang J et al., 2008; Kalmoni et al., 2015; Lui, 2016; Kalmoni et al., 2018). Although these are now thought to be a key element of substorm onset, their observation by spacecraft mounted global auroral imagers has only been reported a few times, e.g. Henderson (2009) as the spatial scales concerned are normally too small to be observed. This highlights the need to study the aurora at a range of spatial and temporal scales, e.g. using SMILE-ASI as described in Section 2.2, and we note that SMILE UVI will have approximately 100 km spatial resolution at apogee and a cadence of 1 minute, which is comparable to previously flown auroral imagers.

An alternative mechanism, or perhaps precursor scenario, suggests that enhanced plasma flows through the lobes (initiated by enhanced dayside reconnection) produce bursts of reconnection in the magnetotail, seen as Bursty Bulk Flows (BBFs) (Angelopoulos et al., 1992) or dipolarizing flux bundles (Liu J et al., 2014) in-situ and as narrow auroral forms aligned approximately north–south, termed "auroral streamers" within the auroral oval. As the magnetotail flows approach the inner magnetosphere, they may create the conditions for the growth of the plasma instabilities associated with auroral beads, initiating the substorm expansion phase activity (Nishimura et al., 2014; Lyons et al., 2021).

Both these phenomena are only observable using ground-based
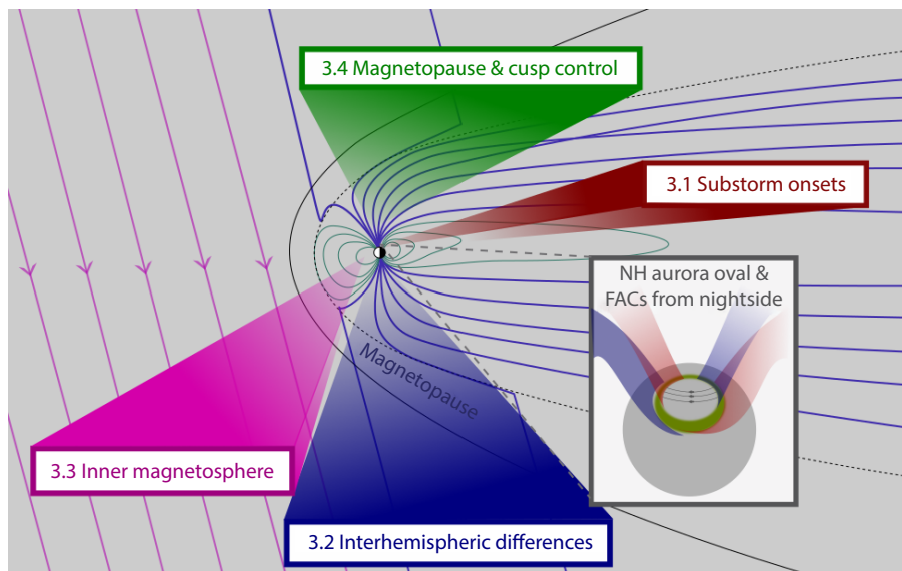
Figure 4.   A schematic of the magnetosphere in the *XZ* plane, where dark blue and green lines indicate magnetic field lines open or closed to the interplanetary magnetic field, respectively. The incoming interplanetary magnetic field is oriented southward in this scenario, shown by pink lines with arrows to the left of the image. The key science areas discussed in this document are highlighted in the text boxes, and refer to Sections 3.1 to 3.4. The inset shows the Northern Hemisphere auroral oval (green) and the upwards (red) and downwards (blue) FACs as seen from the nightside of the Earth.
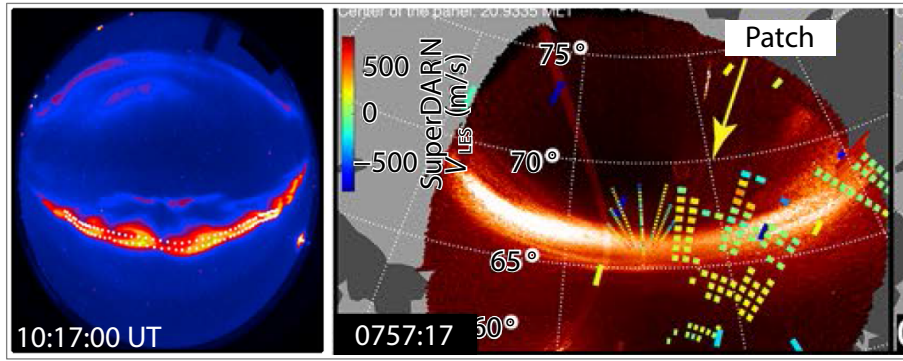
Figure 5.   (Left) Auroral beads (Kalmoni et al., 2017) versus (Right) auroral streamers reaching the main auroral (Lyons et al., 2021), as nightside trigger mechanisms for substorms. Both images originate from ground-based all-sky imagers.

all-sky auroral imagers (ASIs) that detect emissions from the ionosphere at kilometre scales on a cadence of a couple of seconds. In combination with SMILE UVI and SXI images, by using the data from a chain of ASIs stretched over a large land mass such as North America, we will be able to link up the large to the mesoscale. If these ASIs also have some colour selection, e.g., separated red and green line emissions, then an estimation of the energy of the precipitating particles can be made and compared to any available in situ measurements (e.g., Cluster, DMSP). The red line, allowing observations of very faint aurora, will be essential in the calibration of the UVI open-closed field line boundary determination (e.g. the main auroral oval as shown in the right-hand panel of Figure 5), and may also show evidence of low-energy streamers not seen in green line data (Kepko et al., 2009). Renovations and modifications to the existing THEMIS ASI network to create a SMILE ASI network is anticipated across the North American sector in time for the launch of SMILE, as described in Section 2.2.

The utility of simultaneous measurements of BBFs following the commencement of a substorm, using data from high-altitude (Cluster) and low-altitude (Swarm) in situ spacecraft, along with signatures of ground-induced currents detected via magnetometer network (SuperMAG), has been demonstrated (Forsyth et al., 2008; Kronberg et al., 2017; Wei D et al., 2021). Swarm was able to resolve mesoscale structural details of the substorm current wedge. Therefore, in the SMILE era, the chain of events from initiation on the dayside to processes on the nightside can be comprehensively tracked at multiple scales using a combination of space and ground-based experimentation, to determine the fraction of BBFs involved in substorms and any precursor requirements for their occurrence will be determined.

Substorm science will benefit greatly from coordinated in situ measurements as well as observations of the plasma flow in the ionosphere. Recent studies by Wei D et al. (2021) and Dong XC et al. (2023), see Section 3.4, have used measurements from Swarm and Cluster, together with magnetometer ground station coverage, to show that both substorm driven BBFs and storm driven, sporadic magnetic reconnection, which in turn drive FACs into the ionosphere, can be tracked via distributed in situ measurements which are well situated in the magnetosphere. The study by Wei D et al. (2021) was able to show the correlated onset of FACs seen at Cluster and Swarm at the time of arrival of the BBF and dipolarisation fronts at Cluster. The up/down signatures of the FACs were similar at the two locations at low and mid-altitudes, with
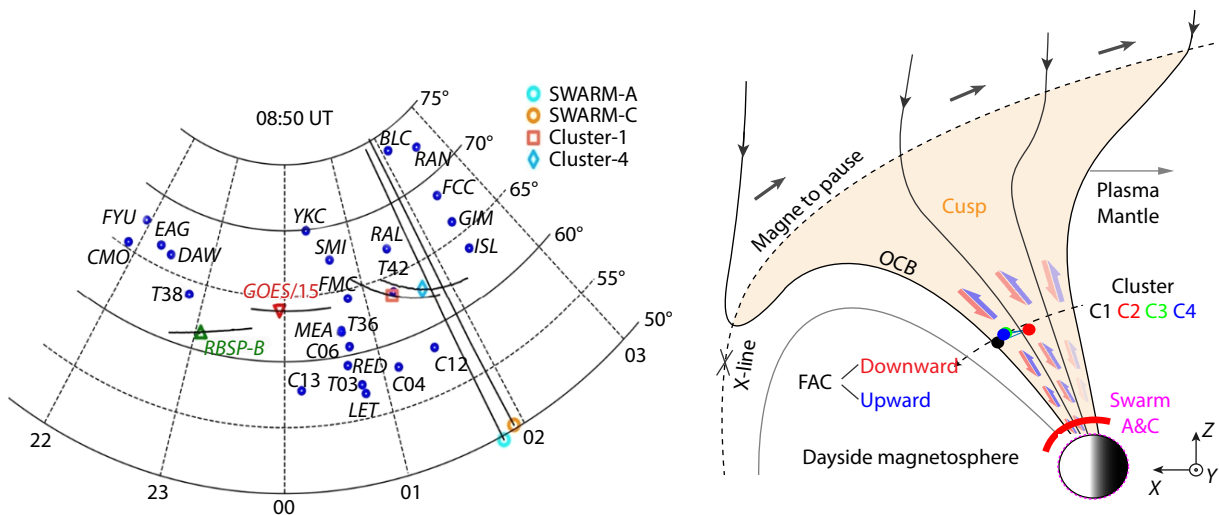
Figure 6.   (Left) The locations of magnetometer ground stations surrounding the satellite tracks of Cluster, Swarm GOES-15 and RBSP-B, mapped along field lines to the ionosphere, for the event studied by Wei D et al. (2021). (Right) Schematic of the locations of the Swarm and Cluster satellites across the cusp throat during the event studied by Dong XC et al. (2023).

Carter JA et al.: Ground-based and additional science support for SMILE

magnetic latitudes (MLAT) corresponding to an L-shell of around 6. The magnetic footprints of the Cluster and Swarm orbits crossed at common MLTs during the intense FAC generation. The ground signatures showed that the most intense rates of change of the horizontal magnetic field perturbation (dH/dt), a proxy for GICs, occurred at the same latitude ($L = 6$) and showed a characteristic reversal in the east component of dH/dt across the conjunction location, consistent with an electrojet (SCW) forming, modified by the addition of a R2 FAC system (Kepko et al., 2015). In fact, the extended array of ground stations shown in the left-hand panel of Figure 6 measure a GIC response which extends to 3.5 of MLT with the most intense dH/dt variations centred around the MLAT of the BBF/DF arrivals. The dipolarisation fronts were also seen by the GOES-15 and RBSP spacecraft, which were located as shown (also at $L = 6$), and the ground perturbations had similar characteristic reversals in the east dH/dt component across the region, confirming the dH/dt pattern, is localise to the FAC sheet. Although the GIC signatures were indirectly driven by the magnetospheric FACs, the study shows that their coupling to the ionospheric induced currents was extremely efficient so that the onset times and locations are common. The arrival of a substorm driven BBF which drives electric currents as seen at Cluster and Swarm into the ionosphere was therefore temporally associated with intense magnetic variations seen by surrounding ground stations.

Furthermore, detailed analysis of the spatial and temporal growth of the aurora, for example by Kalmoni et al. (2018), and the plasma conditions associated with the contemporaneous growth of ultra-low frequency (ULF) waves in the magnetotail, e.g. Smith et al. (2020; 2023) coupled with the global dynamics observed by SMILE may reveal much more about the contributors to the growth of plasma instabilities at substorm onset. In conjunction with SMILE UVI, LIA, and MAG, the combination of other in situ and ASI and ionospheric flow and conductivity measurements, will be a powerful tool in understanding the evolution of a substorm.

3.2 Question 2: What Controls Interhemispheric Differences?

Auroral emissions are an important indicator of magnetospheric structure, dynamics, and state. Until recently it was usually assumed that the auroral morphology in the Northern and Southern hemispheres was roughly conjugate. However, on the rare occasions when simultaneous imaging of the two hemispheres is possible, significant discrepancies are found, e.g. Østgaard et al. (2015). Such discrepancies can be auroral features and emission intensity within the main auroral oval, e.g. Laundal and Østgaard (2009); Østgaard et al. (2018), related to substorm dynamics (e.g., Østgaard et al., 2011a, b; Reistad et al., 2016), or auroral features located at high latitudes, such as transpolar arcs (e.g. Østgaard et al., 2003; Carter et al., 2017; Zhang QH et al., 2020). In the latter case, this may be that transpolar arcs are present in one hemisphere but not the other, or that arcs are present in both hemispheres but are displaced with respect to each other. The formation mechanism for transpolar arcs is still controversial, for instance, are they formed on open or closed field lines? (e.g. Reidy et al., 2017), and investigating the non-/conjugacy of these auroral features is key to understanding their cause. All of these asymmetries indicate

that the coupling of the solar wind with the magnetosphere has introduced a convoluted magnetic topology to the magnetosphere, probably through a combination of poorly understood reconnection geometries at the magnetopause, affected by dipole tilt and the B_x, B_y, and B_z components of the IMF, or reconnection in a twisted magnetotail (e.g., Milan et al., 2005; Østgaard et al., 2011b).

Ionospheric conductivity plays an important role in coupling the magnetosphere and ionosphere. Dipole tilt introduces interhemispheric differences in the distribution of conductivity produced by insolation, and the effect on the conjugacy of M-I coupling is poorly understood. Moreover, the auroral non-conjugacy discussed above will also lead to differences in conductivity produced by precipitation of energetic particles. This affects the magnitude of the field-aligned currents required to transfer momentum from the magnetosphere to the ionosphere (Coxon et al., 2016), which will further contribute to the interhemispheric asymmetry of the auroras. This has technological implications as auroral precipitation, field-aligned currents, and Joule heating, the latter two controlled by conductivity, are major inputs to the energy budget of the two hemispheres, modulating space weather hazards such as satellite drag and geomagnetically induced currents. Knowledge of the spatially variable conductivity is thus important for understanding both M-I coupling and space weather, but often crude models of conductivity are used, parameterized solely by incoming solar wind conditions.

SMILE UVI will be the first global auroral imager in orbit since March 2008, when the NASA Polar satellite ended its mission (Liou, 2010), and hence SMILE UVI will provide, for the first time in two decades, high temporal resolution observations with broad coverage of the polar regions, though with two main caveats. Firstly, it will only image the northern hemisphere. Making use of all available auroral imagers both ground and space-based is essential in the study of inter-hemispheric differences. Secondly, SMILE UVI will only measure auroral emissions in a broad wavelength band (nitrogen emissions from 150 nm to 180 nm), without any spectral selection possible. Using multiple wavelengths, e.g., from the long and short Lyman Hopfield Band emissions at UV or red/green bands in the optical, it is possible to estimate the energy of the incoming precipitating particles that result in the aurora, from which, in turn, the conductivity can be modelled. As it has no wavelength discrimination, SMILE UVI will provide a guide to where conductivity may be high or low.

To overcome these limitations to the SMILE UVI, observations from other sources, on the ground and in space, will be necessary for accurate quantification of conductivity. Current space-borne auroral imagers, such as the SSUSI experiment onboard the DMSP spacecraft, see Section 2.4, does provide wavelength discrimination and can estimate ionospheric conductance, albeit with coarse temporal resolution. Coordinated measurements between SMILE UVI and DMSP/SSUSI will allow extrapolation of the SSUSI observations more globally. Moreover, DMSP/SSUSI samples both the northern and southern hemispheres, so inter-hemispheric studies can be conducted (e.g. Carter et al., 2017). Ground based auroral imagers in the Arctic (including the SMILE-ASI as described in this paper) and Antarctic can provide inter-hemispheric observations

and precipitating energy measurements using red/green filters, at least in winter months, as well as numerous opportunities to check for auroral conjugacy. Ground truth for conductivites can also be provided by contemporaneous measurements with incoherent scatter radar experiments, e.g., EISCAT 3D (McCrea et al., 2015) which will be operational by the time SMILE launches.

As well as auroral emissions, interhemispheric differences in current systems and the control by variable IMF can be observed in the context of both the SMILE imagers and in situ measurements, by using conjugate stations such as those across Greenland and Svalbard along with stations across Antarctica, e.g. Xu Z et al. (2017). In Figure 7 we plot example equivalent ionospheric currents derived from magnetometer data for an event on 5 June 2016, for both the northern and southern hemispheres, showing asymmetries between the hemispheres (J. Wegland, private communication).

3.3 Question 3: What Feedback Role Does the Inner Magnetosphere and Ring Current Play?

The inner magnetosphere is likely to play a significant role in moderating the flow of energy and mass in the magnetosphere and is likely to involve bidirectional feedback to and from the outer magnetosheath. The ring current and radiation belts are thought to be highly time dependent, fed by nightside processes such as ion and electron injections, and drained by loss processes. Plasma plumes are regions of cold and dense equatorial plasma that extend from the inner magnetosphere to the magnetopause, and that have been found to occur under disturbed geomagnetic conditions. Plasma plumes that reach the magnetopause have been shown to modulate magnetic reconnection (Walsh et al., 2014a, b), and produce magnetopause indentations resulting in throat aurora (Han DS, 2019). The formation and evolution, and

hence importance of these plasma plumes is still to be determined. Imaging of mesoscale dynamics on the order of 1 to 3 R_E, within the spatial resolution of SMILE SXI and subsequent auroral by ground ASI, in conjunction with simultaneous in situ measurements, e, g. SMILE, DMSP etc., to quantify ion injections are essential to understand these regions. All the SMILE instruments will help to provide the global context for localised measurements of the ring current and to understand this region.

Recent studies of the in situ ring current (RC) density using MMS data, through application of the curlometer method, show large and small-scale structures and have extended earlier multi-point studies of ring current density with Cluster and THEMIS in terms of the radial and azimuthal coverage (Tan et al. private communication). Figure 8 (left panel) shows the morphology of current density in the RC. This has been shown to be broadly consistent with previous in situ studies in the sense that a strong dawn/dusk and noon/midnight asymmetry is apparent. In particular, a partial RC, or banana current, with an inner eastward current (blue, left panel), could be identified. This is most clearly seen in the noon to dusk quadrant. No evidence of a RC enhancement on the dusk-side during geomagnetic active periods was found, however, and the RC was seen to have a layered structure in latitude. The competing effects of the east–west current directions with radial distance was also observed.

Figure 8 (right panel) shows both FACs measured by MMS adjacent to the RC and subsequently mapped to Swarm altitudes, and dual-satellite Swarm measured FACs ($J_{||}$). This provides an indication that the linkage between RC behaviour and the operation of R2 FACs can be investigated directly. The statistical coverage for the MMS period of RC crossing data shows some overlap between connecting Swarm FACs and parallel currents adjacent to the RC at MMS, predominantly between 60° and 70°. The R2 FACs overlap
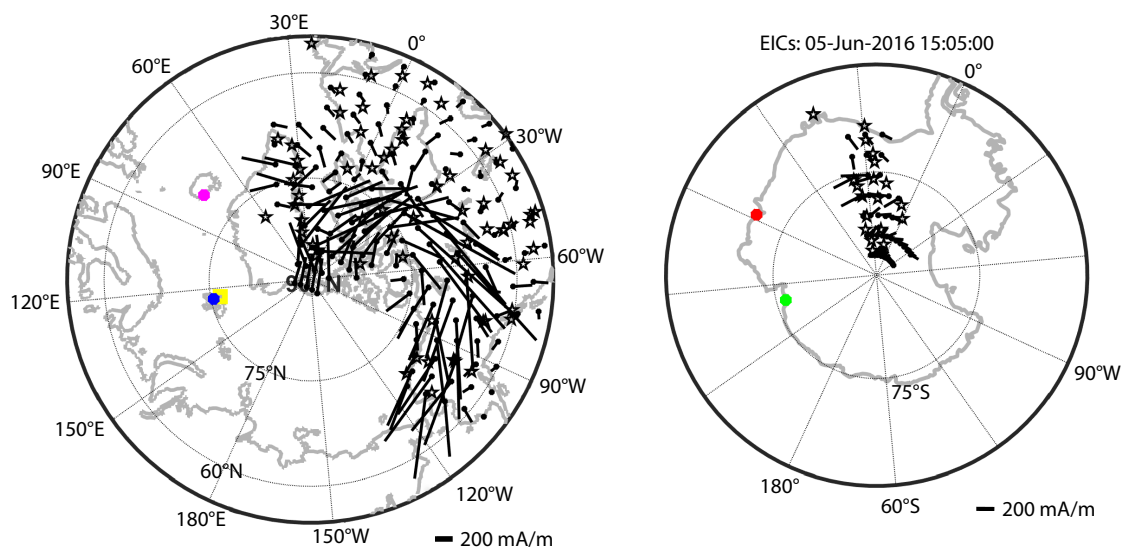
Figure 7.   (Left) Northern and (right) southern hemisphere equivalent ionospheric currents (EIC) for 15:05 UT on 5 June 2016 shown in a magnetic coordinate system with noon at the top of the panel and dusk to the left. The southern hemisphere is shown as a glass earth projection. The top row shows the equivalent ionospheric currents where the dot indicates the position at which the current is determined and the vectors indicates the magnitude (reference vector bottom right) and direction of the current. The squares indicate different stations: Yellow River (yellow), Longyearbyen (blue), Tjornes (mauve), Zhongshan (green), and Syowa (red). Stars indicate ground magnetometer stations with good data for that day.
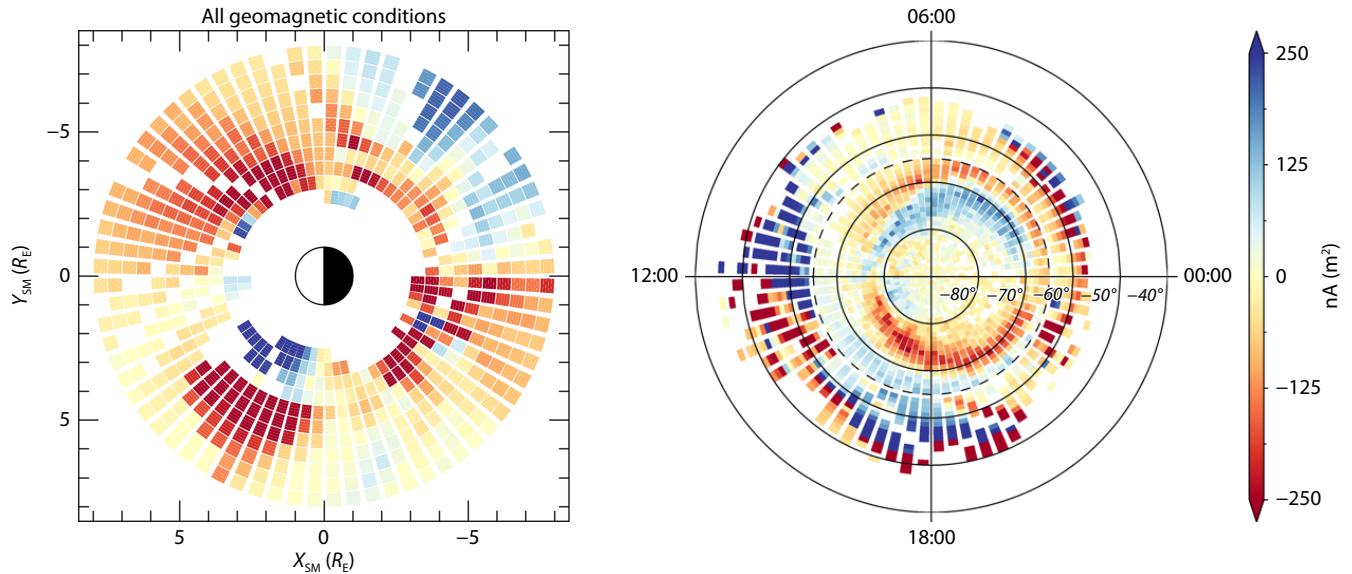
Figure 8. Plots of the morphology of current density in the ring current (left; from J_ϕ) and comparison of FACs (right; from $J_\parallel$), measured both adjacent to the RC and by Swarm in the ionosphere. Note that the $J_\parallel$ current densities from MMS have been scaled in strength to the expected density at Swarm altitudes. This is expected to be an overestimate, by up to a factor of 1.5, particularly for the sub-auroral regions (Tan et al., private communication).

with the RC region for the most part. The FACs adjacent to the RC at MMS are difficult to separate, however, and map to both R1 and R2 depending on the MLAT range. Nevertheless, in the auroral zone (particularly within 65 deg, shown as a dashed circle), they do follow qualitatively the low altitude R1/R2 pattern for the MMS data period. In addition to the direct mapping of the in situ RC signatures, any local-time asymmetry can be compared to modelled RC influences as seen in ground, e.g. by riometers, and low orbit data, and this could contribute to an updated RC index. Therefore, wider MLT coverage at LEO in the (sub-) auroral zone, such as the data collected from the LEO platform magnetometers and future measurements from the two tilted NanoMagSat satellite orbits, will be of benefit to the community.

In conjunction with SMILE, we will investigate RC feedback loops in the magnetosphere in great detail using a combination of space-based, such as described above, and ground-based experimentation. Geomagnetic storms are an enhancement of the RC. Recent work by Walach and Grocott (2019); Walach et al. (2021) has shown how the ionospheric convection pattern responds during geomagnetic storms. In particular, Walach and Grocott (2019) showed that the convection pattern can move to latitudes as low as 40 degrees during geomagnetic storms, which is much lower than previously thought and Walach et al. (2021) showed that the dayside portion of the convection pattern responds strongly to the levels of dayside driving observed during geomagnetic storms. These types of results help us plan for the SMILE mission and give us clues in how the system will respond to high levels of solar wind driving

3.4 Question 4: What Roles do Magnetopause Interactions and the Cusps Play in Moderating the System?

The large-scale magnetospheric dynamics that will be observed by SMILE are primarily driven by its interaction with the solar wind,

which takes place at the magnetopause. When the IMF is southward, magnetic reconnection can occur at the dayside magnetopause, in a manner that appears often to be time-dependent. Whether temporal variations in the reconnection rate are driven by upstream conditions, or inherent to the reconnection process, remains an open question. Magnetopause reconnection leads to a reconfiguration of the Earth's magnetic field, an increase of the open flux content of the polar cap, and an erosion of the magnetopause boundary, which is pushed Earthward. Empirical relations exist that link the overall dayside reconnection rate to upstream solar wind parameters, but what controls the length of the reconnection line and the magnetic flux content of individual bursts of reconnection (called 'flux transfer events') remain key questions of interest. Under northward IMF conditions, reconnection happens at the high-latitude magnetopause adjacent to the magnetotail lobes, resulting in a stirring of the high-latitude ionosphere. The special case of dual-lobe reconnection results in a complicated magnetic topology, and phenomena such as horse-collar aurora (e.g. Milan et al., 2020, and references therein). What controls dual-lobe reconnection and how this feeds the plasma population of the inner magnetosphere is a topic of debate. Furthermore, recent observations have shown the intriguing interplay between lobe reconnection at the high latitude magnetopause and another northward IMF phenomenon, the transpolar arc, which corresponds to a region in which the magnetosphere is closed in an azimuthally-limited region; the implications for the effect of transpolar arcs on lobe reconnection, and vice versa, are yet to be fully explored.

Under both the southward and northward IMF scenarios, solar wind plasma is able to enter the magnetosphere through the cusp regions, in both the high latitude northern and southern hemispheres. This allows for direct entry of solar wind plasma deep into the ionosphere, sending particles along field lines to the

polar regions. The flow of energy, mass, and momentum into the ionosphere from reconnection makes understanding the magnetopause and cusp regions crucial in quantifying the effects of space weather at Earth; the SMILE in situ instruments will monitor the incoming dayside conditions, which can then be linked to auroral phenomena in the cusp region and dayside auroral oval (such as a cusp spot or poleward moving auroral forms). The science of dayside interactions will also be advanced over the next couple of years through NASA's TRACERS mission, and the ongoing measurements provided by SuperDARN (Chisham et al., 2008, Sections 2.1, 2.4).

Detailed measurements of reconnection rates can be achieved through mesoscale measurements of ionospheric convection (e.g. HAIRS, SuperDARN) and the implications in the high-latitude regions can be determined at fine temporal and spatial scales through incoherent scatter. This will allow, for example, investigation of the relationship between upstream solar wind conditions, which are known to control the magnetopause reconnection rate, and the frequency, spatial extent, and flux content of individual bursts of reconnection. Information about the local time extent of individual bursts of reconnection, and their contribution to global magnetic flux transport, will be obtainable by combining their auroral signatures (poleward moving auroral forms; occurring on spatial scales from several 100 km but that can extend to many hours of MLT) and flow signatures (pulsed ionospheric flows), respectively (Milan et al., 2016; Fear et al., 2017), as observed by SMILE UVI imager and ionospheric radars. This is a powerful combination of datasets, as the location of the auroral oval provides information on the location of the open/closed field line boundary which is needed to estimate the dayside/nightside reconnection rates with SuperDARN data. Here, additional datasets are also crucial, as the estimates of the open/closed field line boundary from SMILE UVI images can be cross-checked against independent determinations from the 'spectral width boundary' in SuperDARN backscatter (Chisham and Freeman, 2004; Wild et al., 2004), and the red-line emission in the new SMILE ASI ground-based network (see Section 2.2, above). Specific modes when using the new tuneable SuperDARN radar may be of benefit here for particular events of interest. Furthermore, inter-hemispheric comparison of the ionospheric convection, as observed by SuperDARN radars in the northern and southern hemispheres, can also provide valuable constraints on the spatial extent of the reconnection line (Wild et al., 2003), and the latitudinal location of the reconnection line can be constrained by examining the low-velocity cutoffs in the downward precipitating and mirrored magnetosheath distributions observed by lower altitude spacecraft in the cusps (Trattner et al., 2005), e.g. TRACERS. Finally, the SMILE in situ observations, coupled with data from other upstream spacecraft (e.g. ARTEMIS, THEMIS, and MMS) will also allow comparison with any upstream drivers of modulation (e.g. Wild et al., 2007). The above datasets will therefore enhance the understanding of the magnetopause reconnection process that can be obtained by SMILE through its observation of the auroral signatures of magnetopause reconnection (as seen by UVI), and may be crucial in interpreting magnetosheath structure observed by SXI during reconnection intervals. Ground-based and additional space-based datasets therefore have enormous potential to extend our understanding of the impact of magnetopause coupling on the magnetosphere, beyond what would be possible with SMILE observations alone.

For northward IMF conditions, SMILE UVI observations will be able to identify when high latitude 'lobe' reconnection is occurring at the magnetopause tailward of the cusps through the presence of a 'cusp spot' just poleward of the dayside main auroral oval. By combining UVI observations with the global convection pattern observed by SuperDARN, it will be possible to measure the rate of high-latitude reconnection (Chisham et al., 2004), and to determine whether the high latitude reconnection being observed is occurring in one or both hemispheres, i.e. single or dual lobe reconnection (Imber et al., 2007), which is important in order to understand the topology changes that are (or are not) occurring at the lobe reconnection site. Indeed, SuperDARN observations can indicate that the reconnecting field line topologies can vary with position along the reconnection line, e.g. Bogdanova et al. (2005). Walach et al. (2022) used a historic SuperDARN dataset of convection maps to investigate the asymmetries in convection maps, including the development of convection cells associated with lobe reconnection during northward IMF and enhanced IMF B_y conditions. They showed that filtering for the location of the convection cells, the reverse convection cells can be automatically picked out of SuperDARN data. Reverse convection cells are most likely during short bursts of northward IMF, which is helpful when searching for lobe-reconnection signatures during the SMILE mission. Spacecraft in equatorial orbit (e.g. THEMIS, MMS, and ARTEMIS) will then be able to observe the magnetospheric consequences, e.g. the formation of a magnetosheath boundary layer on the dayside, and cold dense plasmasheet on the nightside in order to better understand the magnetospheric system's response to northward IMF conditions. SMILE UVI observations will also be able to identify intervals when transpolar arcs are present. Given that SMILE will take observations for the majority of its orbital period, it is likely that the spacecraft will make in situ observations as it crosses the high latitude magnetopause; there is therefore the possibility that SMILE will be able to make direct in situ measurements of the interaction between lobe reconnection and transpolar arcs, and the associated field line topology changes. Such an interaction has so far only been inferred from auroral observations (Fear et al., 2015).

Near step-changes in the solar wind dynamic pressure have been shown to rapidly restructure the electrodynamics of the terrestrial magnetospheric–ionospheric system and are known as geomagnetic sudden commencements, e.g. Fogg et al. (2023). A rapid earthward motion of the magnetopause on the order of 1 R_E is anticipated in such cases, within the spatial resolution requirements of SMILE-SXI. Models of sudden commencements may be tested following initiation on the dayside to be observed by SMILE SXI, a fast response in the high-latitude polar cap showing lobe reconnection signatures as observed by SMILE UVI, and accompanying ULF wave signatures to be detected through networks of ground magnetometers.

Favourable dayside crossings from in situ spacecraft (Swarm, DMSP, Cluster) will determine the energy of precipitating particles. A further study showing the coordination of Cluster and Swarm

has been published by Dong XC et al. (2023), which shows common FAC signatures at different heights in the mid and low altitude cusp during storm conditions (see right-hand panel of Figure 6). In the event shown, the Cluster and Swarm arrays fly across the mid and low altitude cusp at different heights, and from high to lower latitudes (MLAT), while they approach a common MLT from either side of noon. The multi-spacecraft Cluster and Swarm measurements reveal matched magnetic perturbations and characteristic FACs (two pairs of up/down currents) at different altitudes simultaneously. At least one magnetometer ground station showed induced signatures during the passage of the satellites through the cusp. Both the magnetic perturbations and the estimated FACs show good agreement between Cluster and Swarm, and are in line with the larger scale relative positions of the Cluster spacecraft, in particular. The simultaneous mesoscale polar cusp, field-aligned currents therefore show vertical scaling and corresponding geomagnetic disturbances. Multiple pairs of opposite FACs in the cusp region are dominant current systems at the dayside during storm time during the arrival of an associated heliospheric current sheet; suggesting these may be caused by unsteady (or pulsed) magnetic reconnection at the magnetopause. Furthermore, the current intensity of these matched FACs decreases from low to high latitude, consistent with the time elapsed since reconnection. The event therefore shows an example of dominant storm driven, dynamic, cusp mesoscale FAC signatures, in contrast to semipermanent, large-scale FACs, suggested to be dominant during quieter times. The study provides further direct evidence for the details of coupling of dayside mesoscale FACs between the magnetosphere, ionosphere and ground in the polar cusp region.

Our direct measurement of the corresponding FACs signals by two Swarm spacecraft provide a further confirmation of this coupling. Compared to the previous Cluster and Swarm conjunction results of Dunlop et al. (2015) and Wei D et al. (2021), which confirmed the matched large scale FACs signals in the ionosphere and magnetosphere, this work is a further extension of them to smaller scale and dynamic cusp FACs structures. Previous observation of the signals of pulsed magnetic reconnection in the ionosphere has mainly been through UVI and radar, which can obtain global features of the injected plasma features. The limitation of the global scale convection picture associated with this kind of pulsed magnetic reconnection in the cusp and the surrounding magnetosphere can therefore be addressed with the SMILE mission (with its UVI and SXI images) in coordination with other in situ measurements. High-latitude ground-based instrumentation such as KHO and the EISCAT Svalbard Radar will provide valuable information whenever data is available.

4. Case studies in the SMILE Era, Under a Variety of Solar Wind and IMF Conditions

Here we discuss generic ground-based studies in the SMILE-era under varying IMF and solar wind conditions, along with one scenario that resulted in a dramatic change in the position of the dayside magnetopause, and the implications this may have at ground-based facilities. The interval of interest for the case study involves the arrival of a solar wind pressure pulse under steady

IMF. These case studies are also being used by the Modelling Working Group (MWG) as part of their preparations for the SMILE mission. The MWG and GBAS teams have considerable overlap and work closely together.

Here we make use of freely available magnetic field-line tracing software, PyGeopack (James, 2023), the location of which is listed in Section 7. The software takes as input the solar wind speed and dynamic pressure, SYM-H index, and IMF B_Y and B_Z components, to trace a field line of the Earth's magnetic field as described by the models of Tsyganenko (2013) (and references therein), at a given date and time. For our modelling, we use a solar wind speed with the only non-zero value to be the X-component, set at -100 km s^{-1}, and the IMF B_Y component is set to zero. The SYM-H value is set to 0.001 nT, and the dipole tilt to 0 for simplicity for these simulations. We find the last closed field line of the magnetosphere in the subsolar region by sampling the field at 351 coordinate points, and we trace this back to the Northern Hemisphere ionosphere, at an altitude of 110 km. The magnetic field model is time dependent, and we use a representative date of 21 June 2025 and a time of 00 UTs. We use the T96 (Tsyganenko, 1995; 1996) model throughout. This method does not use a magnetohydrodynamic model of the magnetosphere that has been primed with simulated solar wind and IMF data prior to our period of interest, however, it does gives us a sense of the scale of the changes observed by SXI as compared to the scale seen by various ground and space-based experiments.

Figure 9a shows an image of the magnetic latitudes of the traced last closed magnetic field lines, ordered by IMF B_Z and solar wind dynamic pressure. The lowest magnetic latitudes are shown by the shorter contours and lighter colours in the bottom right-hand corner of the image, for the most negative IMF B_Z and higher solar wind dynamic pressures. This is as expected following the expanding contracting polar cap model involving an increase of open flux content of the polar cap region under solar wind driven conditions provoking low-latitude dayside reconnection (Milan et al., 2012). In Figure 9b we plot the last closed magnetic field line magnetic latitude as a function of solar wind dynamic pressures. Lines are shown for constant IMF B_Z, where gray lines are for northward IMF ($B_Z > 0$) and the colored lines for southward IMF ($B_Z < 0$). All traces show similar rates of change in magnetic latitude with increasing solar wind pressure. Little change in magnetic latitude is shown between northward IMF cases, when dayside magnetic reconnection is suppressed. In Figure 9c and d we explore the change in L-shell for the last closed magnetic field line, given starting values of IMF B_Z of 0 nT and -5 nT, and solar wind dynamic pressures of 5 nPa and 15 nPa. Changes in parameters and in L-shell are assumed to be instantaneous. We mark on contours for a 0 R_E and a -0.5 R_E change. The 0.5 R_E change is taken from the SMILE SXI science requirements to achieve better than 0.5 R_E accuracy in the magnetopause position after a 5 min integration under solar wind flux of at least 4.9×10^8 cm^{-2} s^{-1} conditions, as described in Section 1. Lower solar wind fluxes will require longer integration times for SXI to achieve this accuracy.

Previous models of magnetopause sub-solar position under changing IMF orientations and dynamic pressures have shown that under constant, low pressures and a southward turning of
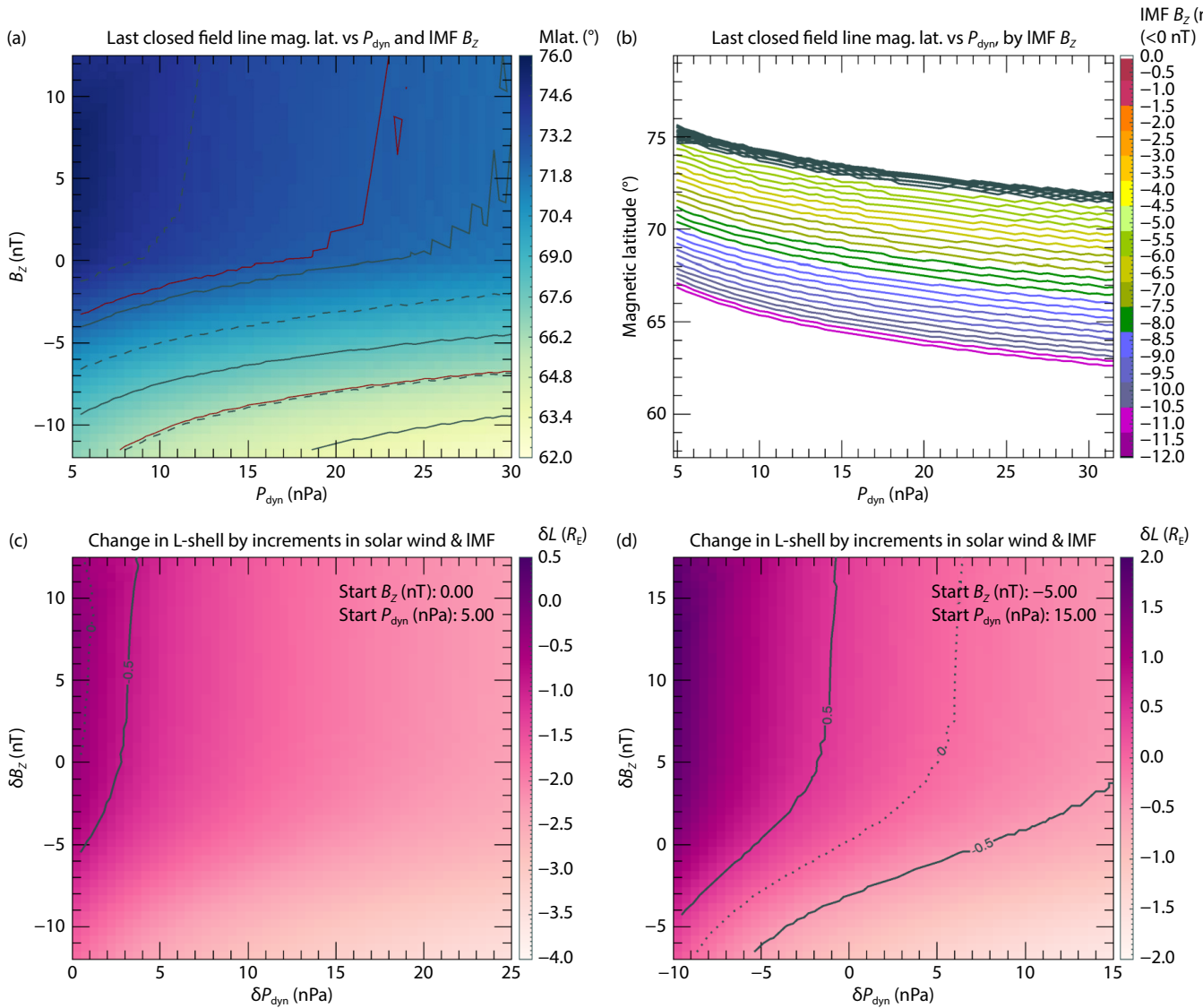
Figure 9. (a) Magnetic latitude of the last closed field line under varying IMF B_Z and solar wind dynamic pressure. Contours, alternatively marked by continuous and dashed lines, are given at 2° steps. Red lines mark example radar magnetic latitudes of Rankin Island (at 72.6°), Stokkseyri (at 66.1°), and Saskatoon (60.9). (b) Magnetic latitude versus solar wind dynamic pressure, for lines of constant IMF B_Z. Colored lines are given for those under southward IMF, where the $B_Z < 0$ nT, as shown by the color bar. Gray lines are under northward IMF. (c) and (d) Changes in L-shell under a change in IMF B_Z and solar wind dynamic pressure, where the starting values are noted in the top right-hand corner. Contours at 0 R_E and −0.5 R_E are marked by the dashed and solid lines.

the IMF, or alternatively under northward IMF and an increase in pressure, a large earthward motion of the magnetopause would be observed (Roelof and Sibeck, 1993). Little change in magnetopause position is observed under constant pressure and a change in orientation of IMF, nor for changes in pressure under constant southward IMF. This is reflected in Figure 9c and d. From these average starting conditions, under constant IMF B_Z, where $\delta B_Z = 0$ nT only a small increase of ~3 nPa dynamic pressure will result in a change of L-shell that is more than the accuracy obtainable by SXI under the conditions and integration time as set out in the science requirements. Under southward, high pressure starting conditions, as shown in Figure 9d, a large change in solar wind dynamic pressure is required to move the magnetopause more than SXI-accuracy requirements, which increases with increasingly northward IMF. It should be noted that the changes observed will

be only a couple of pixels in sequential SXI images for the fast majority of variations in IMF and pressure. This suggests that event orientated studies are likely to be the focus of SMILE-based research, at least initially.

Firstly we consider a northward to southward IMF turning from +5 nT to −5 nT under constant dynamic pressure of 5 nPa, we see from Figure 9a that the last closed field line moves 4° equatorward from 75.5° to 71.5°. Note, this is assumed as an instantaneous shift in the last closed field line, and is used for illustration purposes here. The real nature of the movement of the magnetopause under varying IMF and solar wind conditions is a primary science goal of SMILE. This shift, when apparent in ionospheric phenomena, is easily measurable by the current suite of solar-terrestrial experiments with global coverage. The SuperDARN spatial resolu-

tion is approximately 0.4° at an altitude of 110 km. Should such a shift occur on the nightside, equivalent to a change of 450 km equatorward assuming an auroral altitude of 100 km, the SMILE ASI network will be able to verify the change observed in the open-closed boundary as determined by UVI. This shift is equivalent to a change in L-shell from 9.3 R_E to 8.9 R_E ($\delta L = 0.4\ R_E$) at the subsolar location, which is at the limits of the SXI requirements. The goal of the SMILE mission is to understand and quantify changes in magnetopause position and the subsequent implications at the ionosphere, so we stress that the δL quoted here is for illustration purposes only, and the real change is a major goal of the mission.

We consider a second case of a dayside solar wind pressure pulse from 5 nPa to 20 nPa, under otherwise stable solar wind and IMF conditions with $B_Y = 0$ nT, $B_Z = 5$ nT, the footprint of the last closed field line moves 2.8° equatorward, from 75.5° to 72.2°, which shows a smaller latitudinal change than in the IMF northward to southward shift described above. This change is over an arc length of approximately 310 km, so detectable by the UVI. L-shell change from 9.3 R_E to 7.5 R_E ($\delta L = 1.8\ R_E$). This is a much larger shift in L-shell than in the previous case, and is more than 3 times the $\delta x = 0.5\ R_E$ requirement of SXI. In the third case that the IMF with $B_Z = -5$ nT under a pressure pulse, we find similar shift in magnetic latitude and L-shell, from 71.5° to 68.8°, or approximately 310 km, and from 8.9 R_E to 7.2 R_E ($\delta L = 1.7\ R_E$). Again, this is easily detectable by SXI and UVI, and SuperDARN and SMILE ASI coverage allows these changes to be monitored at ionospheric altitudes.

Carter et al. (2021) examined an interval of extremely high pressure solar wind, under IMF B_Y-dominated conditions associated with a double ICME (16 and 17 June 2012), which compressed the dayside magnetopause and was assciated with observed high-latitude aurora and high-latitude FACs within the polar cap. This interval is also being used by the MWG as part of the preparations for SXI. In this case, the pressure reached 40 nPa at maximum, and exceed 15 nPa for over 5 hours. Region 1 FAC currents were observed in the dayside ionosphere at around 75° at the highest latitude, and large NBZ currents were seen above 80°. A magnetohydrodynamic (MHD) model was used to simulate the interval. The last closed field line was modelled to compress to 6 R_E, before recovering over 8 h later to over 8 R_E. A quick transition of the location of magnetopause magnetic reconnection site was modelled under varying IMF at the shock front of the ICME. SMILE SXI will be able to track and constrain the changing magnetic reconnection for such an interval. Modelled FACs reproduce the observed NBZ FACs reasonably well as these move across the polar cap under changing IMF B_Y, however, the modelled to observed region 1 FACs are discrepant in the later hours of the interval, with the observed region 1 FACs several degrees poleward of those of the model, found at lower latitudes at approximately 70°. This dynamic range in the observed phenomena is well covered by the global SuperDARN and globally distributed magnetometers included in SuperMAG. High-latitude auroral emissions will be observable during winter months by ground-based ASIs, and can be used in conjunction with SMILE-UVI for similar cases to constrain estimates of height-integrated conductances. The Carter et al. (2021) case occurred during Northern Hemisphere summer when conductances due to photoionization

in the northern ionosphere were high. The chain of events from ICME impact from the large scale to monitoring the FAC and auroral response at the ionosphere would have benefitted from the multiscale perspective of lower-altitude spacecraft such as Swarm. Higher cadence auroral observations, such as those from SMILE UVI would have allowed near-continuous monitoring of the cusp aurora during the interval. This interval resulted in a Kp index of 6, however, had the IMF been southward during this impact, then the space weather effects may have been much more severe. Understanding the multiscale, system-wide response to ICMEs is a goal of the spaceweather community, and fits with the primary objectives of the SMILE mission.

5. Community Tools, Strategies, and Data Products

The GBAS WG are developing a set of practical outputs to fully exploit SMILE data. We will leverage experience in various international consortia that have combined space and ground-based data, such as within ECLAT, Cluster, Swarm-Aurora, EISCAT 3D, and SuperDARN. We will also work with other space-based missions, such as Swarm, and EZIE, and we have representation from these missions in the working group.

We have proposed to use Swarm level 1 and 2 data products at a minimum of 1 s cadence to create data products combined with those of the SMILE imaging and in situ instruments. We have begun to develop ideas with the Swarm virtual research service, or VirES, team to link up with their existing data portals.

The data from EZIE will be a set of time-separated 2D maps of the magnetic field and equivalent current constructed from each beam and pointing, from each spacecraft. EZIE has established connections with SuperMAG to determine timings and locations of auroral bulge crossings, and the AUTUMN East–West chain of magnetometers is likely to play a role here too. Auroral imaging here will be of particular importance to verifying the auroral crossings during the progression of a substorm; a technique which is well established in the community but which has unavailable on large scales for many years. SMILE UVI will be of great benefit, given its high cadence and high-resolution global auroral images to further monitor the auroral bulge through the evolution of the substorm.

EISCAT has a long history of working in conjunction with satellite observations, both at the mainland and with the ESR. In recent years notable work has been done with Cluster, SWARM and ARASE, studying aspects of the cusp, substorm flows and auroral structures, such as pulsating auroras. Satellite conjunctions can be planned for and experiment time can be obtained by users in the EISCAT associate countries or by anyone via EISCAT's third party peer review process. In addition, there is a pool of time that is used to regularly support joint-EISCAT-satellite observations, at the moment this is dedicated to SWARM and ARASE, but anyone can present a white paper proposal to the EISCAT science committee to ask for access to this pool of time. SMILE would be an obvious candidate for this route.

There are many ways that SMILE and EISCAT observations can be combined to study exciting new science. The in-situ measurements of SMILE will provide excellent information of the conditions of

the solarwind/magnetosheath and the driving of the magneto-sphere–ionosphere system that EISCAT is observing. The imaging capability of SMILE will be particularly powerful when used in conjunction with EISCAT. One of the major aims of EISCAT_3D science is investigating the multiscale variability of the ionosphere and the imaging provided by SMILE will allow this to be expanded to a much larger scale, beyond simply providing the ionospheric context for the radar measurements. While EISCAT_3D is monitor-ing the auroral zone, the EISCAT Svalbard radar will measure the ionospheric footprint of the cusp, another region that SMILE will be imaging. Taken all together, along with the many other excellent ground-based instruments that populate the area around EISCAT there is a real opportunity to provide comprehensive multiscale studies of space weather phenomena.

We are also working on the best strategies for assisting SMILE in its main science objectives. The highest scientific return is expected in winter months, when ground-based optical data are available in the high-latitude polar regions of the northern hemi-sphere, e.g. Svalbard. New-moon period observations are desirable for both dayside and nightside auroral viewing. Nightside coverage of the substorm auroral oval will be optimal for the SMILE-ASI and other Northern American imagers from 06:00 to 12:00 UT. We are working with the SuperDARN and EISCAT consortia to consider which radar operational modes will be best, and designing new modes if desirable, for coordinated observing campaigns with SMILE. We are preparing for new-moon campaigns, in collaboration with KHO, EISCAT, and EISCAT_3D, to be ready for the first winter of SMILE science operations.

We have begun a SMILE Data Fusion Facility (DFF) to fuse SMILE SXI and UVI data with ground-based facilities data, in particular global ionospheric convection maps from SuperDARN and magnetic perturbations from the SuperMAG chain. We also provide a Conjunction Planning tool, which uses the SMILE satellite orbital ephemerides, to aid in preparing for SMILE conjunctions and the timely optimisation of ground-based experiments, e.g. radars being set in special modes. Data availability graphics are included so that a user may chose data with a minimum threshold of points or a maximum SXI integration time. A link to the current facility is found in Section 7 below. The development of this DFF is ongoing, and requires an iterative approach between applying updates from feedback received through consultation within the GBAS WG and wider community representatives. This facility is currently populated with a limited sample of ground-based data with dates adjusted to the mission operational phase based on an earlier expected launch date than is currently anticipated, along with simulated SXI data. Other data sets, such as from the AUTUMN magnetometer network, particularly from the Northern Hemisphere, may be incorporated into the DFF when appropriate. It is not intended that the DFF include all ground-based data that has so far expressed support for SMILE, but that the data included are carefully chosen to provide the most useful resource to the widest community. The DFF is written with the idea that it is intu-itive, and optmised for ease of use by the maximum number of scientists.

In Figure 10 we plot examples from the SMILE DFF. In (a) we show an example of the combined data or fusion plot, where both the

SXI-derived magnetopause and ground-based data from the Northern Hemisphere is presented simultaneously. One of the SXI Level 4 products will be parameters to describe the magnetopause three-dimensional shape, determined from forward-modelling techniques applied to the SXI image. The derived magnetopause location in the subsolar region is traced back along a magnetic field line to a northern hemisphere ionospheric footprint for a user specified date and time, and plotted on a magnetic latitude, magnetic local time grid as the purple line in this panel. The magnetic field line model used for this tracing is dependent on contemporaneous solar wind and IMF conditions. A user of the DFF can select either archived (OMNI, King and Papitashvili, 2005) solar wind and IMF data, or their own desired parameter values as input to this model. Similarly, a user may chose between several Earth magnetic field models (see the review of models in Tsyga-nenko (2013)) for the tracing. The methods to derive the magne-topause location and shape from the two-dimensional SXI images are under investigation by the MWG, e.g. Collier and Connor (2018); Jorgensen et al. (2019, 2022); Samsonov et al. (2022). The method used at any date and time selection made by a user of the DFF will be clearly identifiable by metadata in the downloadable fusion products. In a similar manner, SMILE ephemerides data is used to field-line trace the spacecraft footprint back to northern ionosphere (dark red line with arrows). The SuperDARN data shown are convection maps of the Northern Hemisphere, and a user may wish to plot either line-of-sight or fitted velocity vectors, coloured by speed. The Heppner Maynard boundary is shown by the green line, and contours of electrostatic potential are shown in grey. SuperMAG fitted vectors can also be plotted on the right-hand panel, scaled in magnitude to the representative 300 nT line shown in the top left. The insert on the right-hand panel shows information that appears when hovering over a SuperDARN or SuperMAG vector. This tool-tip option can be turned-off as part of various plotting options that appear above either panel. Output from the fusion section can be in the form of images, Flexible Image Transport System (FITS) files or Network Common Data Format (netCDF) files. The FITS files combine the data using various file extensions for each data set appended to the original SXI Level 4 magnetopause fitting result used in the plot.

In Figure 10b we plot an example from the Conjunction Planning section of the DFF. Here, fields of view of the SuperDARN radar are shown on a Northern Hemisphere magnetic latitude, MLT grid, for a user-specified date-time. SMILE ephemeris data is used to field-line trace the spacecraft footprint to the ionosphere, when a solu-tion is found in magnetospheric model. The field-line tracing options are the same as for the fusion section described above. We also intend to add the field-of-view of other facilities to this section, e.g. EISCAT 3D. Output from this section can be down-loaded as an image, or an ASCII file listing the approximate times the spacecraft field-line footprint spends in a radar's field of view.

In Figure 10c we show the Advanced Options panel detailing how users can specify various solar wind, IMF, and model parameters of choice, for both the DFF visualisation and Conjunction Planning sections.

In Figure 10d we show a data availability trace that is plotted above the SXI image and northern hemisphere ionosphere panels
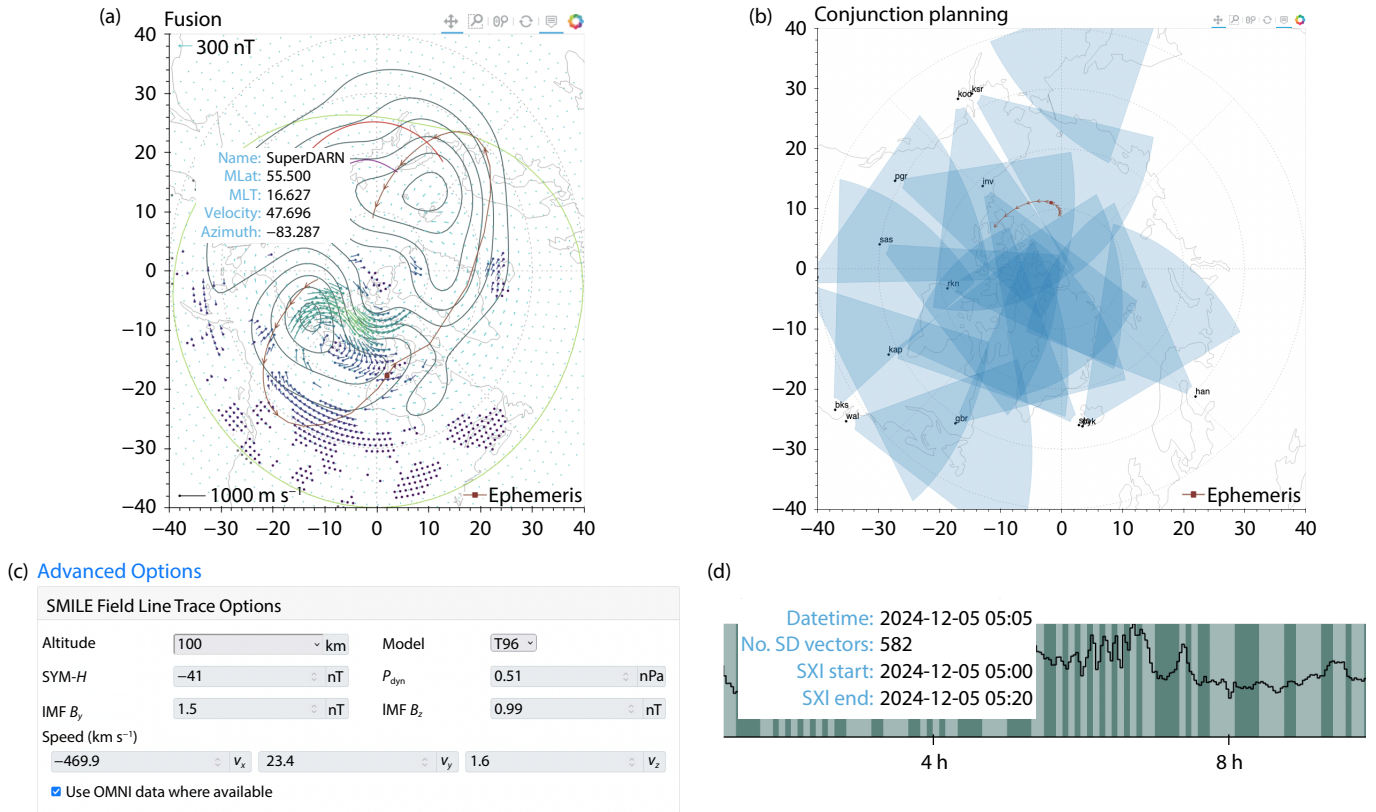
Figure 10. SMILE SXI simulation and DFF illustrations. The DFF is under construction and so corrections and adaptations are in the process of being applied following community consultation. (a) DFF visualisation of real data-shifted SuperDARN and SuperMAG data with derived SXI results, co-located on a Northern Hemisphere magnetic latitude, MLT grid. We show example tool-tip activated information about one particular vector. Various features plotting options are available with the visualisation window, as described in the main text. (b) Part of the Conjunction Planning section of the DFF, to allow for joint ground-SMILE observation optimisation. (c) Advanced options panel for field line tracing in both the DFF visualisation and conjunction panels, see (a, b). (d) Data availability trace for the DFF visualisation section, showing alternate SXI integrations coloured either light or dark green, and the number of SuperDARN vectors used to produce each map in the black trace.

of the DFF visualisation. The trace shows the number of fitted SuperDARN vectors, which is often used as a measure of quality for a convection map. Coloured areas show the integrated time periods used to construct each available SXI image, and these are coloured alternatively between light and dark green to aid the eye.

We intend to make all GBAS WG data products available through principal investigating research institutions and also to ingest these products into the ESA SMILE archive, if assessed as suitable by the wider SMILE Consortium. So far along the mission timeline, even with the limited time and resources we have been able to dedicate to the preparations for SMILE, we have demonstrated considerable potential for SMILE science exploitation from the ground-based and wider solar-terrestrial community.

6. Conclusions

We have described the wide variety of experiments that have, to date, expressed support for the SMILE mission. We have shown that these supporting experiments will greatly enhanced SMILE's main mission goals. In conjunction with observations and measurements from SMILE, these experiments will gain new and detailed insights into outside scientific questions in the field. We

have also described our efforts to prepare for the practical aspects of combining SMILE data with these other experiments.

Solar terrestrial physics uses instrumentation that bridges tradi-tional research agency boundaries, given the range of space-based and ground-based experiments to give a holistic view of the Earth's magnetosphere. The cross-disciplinary science aims of SMILE are its strength, and we urge national research councils to facilitate embedding the ground-based segment into their plans for the SMILE mission now.

7. Open Research

This work makes use of the PyGeopack magnetic field line tracing software: https://github.com/mattkjames7/PyGeopack. The SMILE Data Fusion Facility can be found at: https://www403.lamp.le.ac.uk/. SuperDARN data can be found via data repositories such as: vt.superdarn.org. SuperMAG data can be found via: supermag.jhuapl.edu. The ECLAT data set can be found through the Cluster Science Archive: https://csa.esac.esa.int/csa-web/. OMNI data used can be found via: https://omniweb.gsfc.nasa.gov/. IMAGE data can be found at https://space.fmi.fi/image and MIRACLE data at https://space.fmi.fi/MIRACLE. ALIS4D data can be found at https://alis4d.irf.se/. EISCAT data can be accessed via https://eiscat.se. KHO data can be accessed via http://kho.unis.no. Svalbard All-Sky

Imager Data is available from: http://tid.uio.no/plasma/aurora/. Swarm-Aurora data can be found at https://swarm-aurora.com/. Information regarding recent updates to SuperDARN radar can be found at https://borealis.readthedocs.io/en/latest/. Coherent scatter radar from the northern Russian region can be obtained on request from http://en.iszf.irk.ru/Main_Page. The ESA report on Swarm can be found at https://eo4society.esa.int/wp-content/uploads/2021/11/swarm_report_211112.pdf. TREx data can be found at https://data.phys.ucalgary.ca/.

Acknowledgments

References

Amm, O., and Viljanen, A. (1999). Ionospheric disturbance magnetic field continuation from the ground to the ionosphere using spherical elementary current systems. *Earth, Planets Space*, 51(6), 431–440. https://doi.org/10.1186/BF03352247

Amm, O., Donovan, E. F., Frey, H., Lester, M., Nakamura, R., Wild, J. A., Aikio, A., Dunlop, M., Kauristie, K., … Strømme, A. (2005). Coordinated studies of the geospace environment using Cluster, satellite and ground-based data: an interim review. *Ann. Geophys.*, 23(6), 2129–2170. https://doi.org/10.5194/angeo-23-2129-2005

Amm, O., Fujii, R., Vanhamäki, H., Yoshikawa, A., and Ieda, A. (2013). General solution for calculating polarization electric fields in the auroral ionosphere and application examples. *J. Geophys. Res.: Space Phys.*, 118(5), 2428–2437. https://doi.org/10.1002/jgra.50254

Anderson, B. J., Takahashi, K., and Toth, B. A. (2000). Sensing global Birkeland currents with iridium® engineering magnetometer data. *Geophys. Res. Lett.*, 27(24), 4045–4048. https://doi.org/10.1029/2000GL000094

Angelopoulos, V., Baumjohann, W., Kennel, C. F., Coroniti, F. V., Kivelson, M. G., Pellat, R., Walker, R. J., Lühr, H., and Paschmann, G. (1992). Bursty bulk flows in the inner central plasma sheet. *J. Geophys. Res.: Space Phys.*, 97(A4), 4027–4039. https://doi.org/10.1029/91JA02701

Angelopoulos, V. (2008). The THEMIS mission. *Space Sci. Rev.*, 141(1-4), 5–34. https://doi.org/10.1007/s11214-008-9336-1

Bahcivan, H., Tsunoda, R., Nicolls, M., and Heinselman, C. (2010). Initial ionospheric observations made by the new Resolute incoherent scatter radar and comparison to solar wind IMF. *Geophys. Res. Lett.*, 37(15), L15103. https://doi.org/10.1029/2010GL043632

Baker, D. N., Stauning, P., Hones, E. W. Jr., Higbie, P. R., and Belian, R. D. (1981). Near-equatorial, high-resolution measurements of electron precipitation at L ≃ 6.6. *J. Geophys. Res.: Space Phys.*, 86(A4), 2295–2313. https://doi.org/10.1029/JA086iA04p02295

Bogdanova, Y. V., Marchaudon, A., Owen, C. J., Dunlop, M. W., Frey, H. U., Wild, J. A., Fazakerley, A. N., Klecker, B., Davies, J. A., and Milan, S. E. (2005). On the formation of the high-altitude stagnant cusp: cluster observations. *Geophys. Res. Lett.*, 32(12), L12101. https://doi.org/10.1029/2005GL022813

Branduardi-Raymont, G., Wang, C., Escoubet, C. P., Adamovic, M., Agnolon, D., Berthomier, M., Carter, J. A., Chen, W., Colangeli, L., … Zhu, Z. (2018). Smile definition study report (red book). ESA. https://doi.org/10.5270/esa.smile.definition_study_report-2018-12

Carlson, H. C., Moen, J., Oksavik, K., Nielsen, C. P., McCrea, I. W., Pedersen, T. R., and Gallop, P. (2006). Direct observations of injection events of subauroral plasma into the polar cap. *Geophys. Res. Lett.*, 33(5), L05103. https://doi.org/10.1029/2005GL025230

Carter, J., Walach, M. T., and Mooney, M. (2022). RAS specialist discussion meeting report. *Astron. Geophys.*, 63(4), 4.38–4.42. https://doi.org/10.1093/astrogeo/atac054

Carter, J. A., Milan, S. E., Fear, R. C., Walach, M. T., Harrison, Z. A., Paxton, L. J., and Hubert, B. (2017). Transpolar arcs observed simultaneously in both hemispheres. *J. Geophys. Res.: Space Phys.*, 122(6), 6107–6120. https://doi.org/10.1002/2016JA023830

Carter, J. A., Samsonov, A. A., Milan, S. E., Branduardi-Raymont, G., Ridley, A. J., Paxton, L. J., Anderson, B. J., Waters, C. L., and Edwards, T. (2021). Field-aligned current during an interval of Bγ-dominated interplanetary-field; modeled-to-observed comparisons. *J. Geophys. Res.: Space Phys.*, 126(12), e2021JA029722. https://doi.org/10.1029/2021JA029722

Carter, J. A. (2022). Earth's exospheric X-ray emissions. In C. Bambi, et al. (Eds.), *Handbook of X-Ray and Gamma-Ray Astrophysics* (pp. 1-27). Singapore: Springer. https://doi.org/10.1007/978-981-16-4544-0_75-1

Chisham, G., and Freeman, M. P. (2004). An investigation of latitudinal transitions in the SuperDARN Doppler spectral width parameter at different magnetic local times. *Ann. Geophys.*, 22(4), 1187–1202. https://doi.org/10.5194/angeo-22-1187-2004

Chisham, G., Freeman, M., Coleman, I. J., Pinnock, M., Hairston, M. R., Lester, M., and Sofko, G. (2004). Measuring the dayside reconnection rate during an interval of due northward interplanetary magnetic field. *Ann. Geophys.*, 22(12), 4243–4258. https://doi.org/10.5194/angeo-22-4243-2004

Chisham, G., Lester, M., Milan, S. E., Freeman, M. P., Bristow, W. A., Grocott, A., McWilliams, K. A., Ruohoniemi, J. M., Yeoman, T. K., … Walker, A. D. M. (2007). A decade of the Super Dual Auroral Radar Network (SuperDARN): scientific achievements, new techniques and future directions. *Surv. Geophys.*, 28(1), 33–109. https://doi.org/10.1007/s10712-007-9017-8

Chisham, G., Freeman, M. P., Abel, G. A., Lam, M. M., Pinnock, M., Coleman, I. J., Milan, S. E., Lester, M., Bristow, W. A., … Villain, J. P. (2008). Remote sensing of the spatial and temporal structure of magnetopause and magnetotail reconnection from the ionosphere. *Rev. Geophys.*, 46(1), RG1004. https://doi.org/10.1029/2007RG000223

Clauer, C. R., Kim, H., Deshpande, K., Xu, Z., Weimer, D., Musko, S., Crowley, G., Fish, C., Nealy, R., … Ridley, A. J. (2014). An autonomous adaptive low-power instrument platform (AAL-PIP) for remote high-latitude geospace data collection. *Geosci. Instrum. Methods Data Syst.*, 3(2), 211–227. https://doi.org/10.5194/gi-3-211-2014

Collier, M. R., and Connor, H. K. (2018). Magnetopause surface reconstruction from tangent vector observations. *J. Geophys. Res.: Space Phys.*, 123(12), 10189–10199. https://doi.org/10.1029/2018JA025763

Connors, M., Schofield, I., Reiter, K., Chi, P. J., Rowe, K. M., and Russell, C. T. (2016). The AUTUMNX magnetometer meridian chain in Québec, Canada. *Earth Planet. Space*, 68(1), 2. https://doi.org/10.1186/s40623-015-0354-4

Coxon, J. C., Milan, S. E., Clausen, L. B. N., Anderson, B. J., and Korth, H. (2014). The magnitudes of the regions 1 and 2 Birkeland currents observed by AMPERE and their role in solar wind-magnetosphere-ionosphere coupling. *J. Geophys. Res.: Space Phys.*, 119(12), 9804–9815. https://doi.org/10.1002/2014JA020138

Coxon, J. C., Milan, S. E., Carter, J. A., Clausen, L. B. N., Anderson, B. J., and Korth, H. (2016). Seasonal and diurnal variations in AMPERE observations of the

Birkeland currents compared to modeled results. *J. Geophys. Res.: Space Phys.*, *121*(5), 4027–4040. https://doi.org/10.1002/2015JA022050

Dong, X. C., Dunlop, M. W., Xiao, C., Wei, D., Wang, T. Y., and Zhao, J. S. (2023). Simultaneous mesoscale polar cusp field-aligned currents measured on mid- and low-altitude satellites. *Geophys. Res. Lett.*, *50*(1), e2022GL102460. https://doi.org/10.1029/2022GL102460

Donovan, E., Mende, S., Jackel, B., Frey, H., Syrjäsuo, M., Voronkov, I., Trondsen, T., Peticolas, L., Angelopoulos, V., … Connors, M. (2006a). The THEMIS all-sky imaging array—system design and initial results from the prototype imager. *J. Atmos. Solar-Terrestrial Phys.*, *68*(13), 1472–1487. https://doi.org/10.1016/j.jastp.2005.03.027

Donovan, E., Mende, S. B., Jackel, B., Syrjäsuo, M., Meurant, M., Voronkov, I., Frey, H. U., Angelopoulos, V., and Connors, M. (2006b). The azimuthal evolution of the substorm expansive phase onset aurora. In *Proceedings of the 8th International Conference on Substorms* (pp. 50-60). Canada: National Research Council (Canada) Press.

Dunlop, M. W., Yang, J. Y., Yang, Y. Y., Xiong, C., Lühr, H., Bogdanova, Y. V., Shen, C., Olsen, N., Zhang, Q. H., … Haagmans, R. (2015). Simultaneous field-aligned currents at swarm and cluster satellites. *Geophys. Res. Lett.*, *42*(10), 3683–3691. https://doi.org/10.1002/2015GL063738

Dunlop, M. W., and Lühr, H. (2020). Ionospheric Multi-Spacecraft Analysis Tools. Cham: Springer. https://doi.org/10.1007/978-3-030-26732-2

Dunlop, M. W., Dong, X. C., Wang, T. Y., Eastwood, J. P., Robert, P., Haaland, S., Yang, Y. Y., Escoubet, P., Rong, Z. J., … De Keyser, J. (2021). Curlometer technique and applications. *J. Geophys. Res.: Space Phys.*, *126*(11), e2021JA029538. https://doi.org/10.1029/2021JA029538

Engebretson, M. J., Simms, L. E., Pilipenko, V. A., Bouayed, L., Moldwin, M. B., Weygand, J. M., Hartinger, M. D., Xu, Z. H., Clauer, C. R., … Gerrard, A. J. (2022). Geomagnetic disturbances that cause GICs: investigating their interhemispheric conjugacy and control by IMF orientation. *J. Geophys. Res.: Space Phys.*, *127*(10), e2022JA030580. https://doi.org/10.1029/2022JA030580

Escoubet, C. P., Fehringer, M., and Goldstein, M. (2001). *Introduction* the cluster mission. *Ann. Geophys.*, *19*(10-12), 1197–1200. https://doi.org/10.5194/angeo-19-1197-2001

Fear, R. C., Milan, S. E., Carter, J. A., and Maggiolo, R. (2015). The interaction between transpolar arcs and cusp spots. *Geophys. Res. Lett.*, *42*(22), 9685–9693. https://doi.org/10.1002/2015GL066194

Fear, R. C., Trenchi, L., Coxon, J. C., and Milan, S. E. (2017). How much flux does a flux transfer event transfer?. *J. Geophys. Res.: Space Phys.*, *122*(12), 12310–12327. https://doi.org/10.1002/2017JA024730

Fear, R. C. (2022). Joint cluster/ground-based studies in the first 20 years of the cluster mission. *J. Geophys. Res.: Space Phys.*, *127*(8), e2021JA029928. https://doi.org/10.1029/2021JA029928

Fogg, A. R., Lester, M., Yeoman, T. K., Carter, J. A., Milan, S. E., Sangha, H. K., Elsden, T., Wharton, S. J., James, M. K., … Vines, S. K. (2023). Multi-instrument observations of the effects of a solar wind pressure pulse on the high latitude ionosphere: a detailed case study of a geomagnetic sudden impulse. *J. Geophys. Res.: Space Phys.*, *128*(3), e2022JA031136. https://doi.org/10.1029/2022JA031136

Forsyth, C., Lester, M., Cowley, S. W. H., Dandouras, I., Fazakerley, A. N., Fear, R. C., Frey, H. U., Grocott, A., Kadokura, A., … Watermann, J. (2008). Observed tail current systems associated with bursty bulk flows and auroral streamers during a period of multiple substorms. *Ann. Geophys.*, *26*(1), 167–184. https://doi.org/10.5194/angeo-26-167-2008

Forsyth, C., Sergeev, V. A., Henderson, M. G., Nishimura, Y., and Gallardo-Lacourt, B. (2020). Physical processes of meso-scale, dynamic auroral forms. *Space Sci. Rev.*, *216*(4), 46. https://doi.org/10.1007/s11214-020-00665-y

Friis-Christensen, E., Lühr, H., Knudsen, D., and Haagmans, R. (2008). *Swarm*-an earth observation mission investigating geospace. *Adv. Space Res.*, *41*(1), 210–216. https://doi.org/10.1016/j.asr.2006.10.008

Gillies, R. G., van Eyken, A., Spanswick, E., Nicolls, M., Kelly, J., Greffen, M., Knudsen, D., Connors, M., Schutzer, M., … Donovan, E. (2016). First observations from the RISR-C incoherent scatter radar. *Radio Sci.*, *51*(10), 1645–1659. https://doi.org/10.1002/2016RS006062

Gjerloev, J. W. (2012). The supermag data processing technique. *J. Geophys. Res.: Space Phys.*, *117*(A9), A09213. https://doi.org/10.1029/2012JA017683

Gjerloev, J. W., and Hoffman, R. A. (2014). The large-scale current system during

auroral substorms. *J. Geophys. Res.: Space Phys.*, *119*(6), 4591–4606. https://doi.org/10.1002/2013JA019176

Han, D. S. (2019). Ionospheric polarization electric field guiding magnetopause reconnection: a conceptual model of throat aurora. *Sci. China Earth Sci.*, *62*(12), 2099–2105. https://doi.org/10.1007/s11430-019-9358-8

Hargreaves, J. K., Chivers, H. J. A., and Axford, W. I. (1975). The development of the substorm in auroral radio absorption. *Planet. Space Sci.*, *23*(6), 905–911. https://doi.org/10.1016/0032-0633(75)90177-4

Henderson, M. G. (2009). Observational evidence for an inside-out substorm onset scenario. *Ann. Geophys.*, *27*(5), 2129–2140. https://doi.org/10.5194/angeo-27-2129-2009

Imber, S. M., Milan, S. E., and Hubert, B. (2007). Observations of significant flux closure by dual lobe reconnection. *Ann. Geophys.*, *25*(7), 1617–1627. https://doi.org/10.5194/angeo-25-1617-2007

James, M. K. (2023). PyGeopack (v1.1.7). Zenodo. https://doi.org/10.5281/zenodo.7688085

Jorgensen, A. M., Sun, T. R., Wang, C., Dai, L., Sembay, S., Wei, F., Guo, Y. H., and Xu, R. L. (2019). Boundary detection in three dimensions with application to the SMILE mission: the effect of photon noise. *J. Geophys. Res.: Space Phys.*, *124*(6), 4365–4383. https://doi.org/10.1029/2018JA025919

Jorgensen, A. M., Xu, R., Sun, T., Huang, Y., Li, L., Dai, L., and Wang, C. (2022). A theoretical study of the tomographic reconstruction of magnetosheath X-ray emissions. *J. Geophys. Res.: Space Phys.*, *127*(4), e2021JA029948. https://doi.org/10.1029/2021JA029948

Kalmoni, N. M. E., Rae, I. J., Watt, C. E. J., Murphy, K. R., Forsyth, C., and Owen, C. J. (2015). Statistical characterization of the growth and spatial scales of the substorm onset arc. *J. Geophys. Res.: Space Phys.*, *120*(10), 8503–8516. https://doi.org/10.1002/2015JA021470

Kalmoni, N. M. E., Rae, I. J., Murphy, K. R., Forsyth, C., Watt, C. E. J., and Owen, J. (2017). Statistical azimuthal structuring of the substorm onset arc: implications for the onset mechanism. *Geophys. Res. Lett.*, *44*(5), 2078–2087. https://doi.org/10.1002/2016GL071826

Kalmoni, N. M. E., Rae, I. J., Watt, C. E. J., Murphy, K. R., Samara, M., Michell, R. G., Grubbs, G., and Forsyth, C. (2018). A diagnosis of the plasma waves responsible for the explosive energy release of substorm onset. *Nat. Commun.*, *9*(1), 4806. https://doi.org/10.1038/s41467-018-07086-0

Kavanagh, A. J., Wild, J. A., and Honary, F. (2009). Observations of omega bands using an imaging riometer. *Ann. Geophys.*, *27*(11), 4183–4195. https://doi.org/10.5194/angeo-27-4183-2009

Kepko, L., Spanswick, E., Angelopoulos, V., Donovan, E., McFadden, J., Glassmeier, K. H., Raeder, J., and Singer, H. J. (2009). Equatorward moving auroral signatures of a flow burst observed prior to auroral onset. *Geophys. Res. Lett.*, *36*(24), L24104. https://doi.org/10.1029/2009GL041476

Kepko, L., McPherron, R. L., Amm, O., Apatenkov, S., Baumjohann, W., Birn, J., Lester, M., Nakamura, R., Pulkkinen, T. I., and Sergeev, V. (2015). Substorm current wedge revisited. *Space Sci. Rev.*, *190*(1), 1–46. https://doi.org/10.1007/s11214-014-0124-9

King, J. H., and Papitashvili, N. E. (2005). Solar wind spatial scales in and comparisons of hourly Wind and ACE plasma and magnetic field data. *J. Geophys. Res.: Space Phys.*, *110*(A2), A02104. https://doi.org/10.1029/2004JA010649

Kronberg, E. A., Grigorenko, E. E., Turner, D. L., Daly, P. W., Khotyaintsev, Y., and Kozak, L. (2017). Comparing and contrasting dispersionless injections at geosynchronous orbit during a substorm event. *J. Geophys. Res.: Space Phys.*, *122*(3), 3055–3072. https://doi.org/10.1002/2016JA023551

Laundal, K. M., and Østgaard, N. (2009). Asymmetric auroral intensities in the Earth's Northern and Southern hemispheres. *Nature*, *460*(7254), 491–493. https://doi.org/10.1038/nature08154

Liang, J., Donovan, E. F., Liu, W. W., Jackel, B., Syrjäsuo, M., Mende, S. B., Frey, H. U., Angelopoulos, V., and Connors, M. (2008). Intensification of preexisting auroral arc at substorm expansion phase onset: wave-like disruption during the first tens of seconds. *Geophys. Res. Lett.*, *35*(17), L17S19. https://doi.org/10.1029/2008GL033666

Liou, K. (2010). Polar ultraviolet imager observation of auroral breakup. *J. Geophys. Res.: Space Phys.*, *115*(A12), A12219. https://doi.org/10.1029/2010JA015578

Little, C. G., and Leinbach, H. (1959). The riometer-A device for the continuous measurement of ionospheric absorption. *Proc. IRE*, *47*(2), 315–320. https://

doi.org/10.1109/JRPROC.1959.287299

Liu, J., Angelopoulos, V., Zhou, X. Z., and Runov, A. (2014). Magnetic flux transport by dipolarizing flux bundles. *J. Geophys. Res.: Space Phys.*, *119*(2), 909–926. https://doi.org/10.1002/2013JA019395

Lockwood, M., Moen, J., van Eyken, A. P., Davies, J. A., Oksavik, K., and McCrea, I. W. (2005). Motion of the dayside polar cap boundary during substorm cycles: I. Observations of pulses in the magnetopause reconnection rate. *Ann. Geophys.*, *23*(11), 3495–3511. https://doi.org/10.5194/angeo-23-3495-2005

Lui, A. T. Y. (2016). Cross-field current instability for auroral bead formation in breakup arcs. *Geophys. Res. Lett.*, *43*(12), 6087–6095. https://doi.org/10.1002/2016GL069892

Lyons, L. R., Nishimura, Y., Donovan, E., and Angelopoulos, V. (2013). Distinction between auroral substorm onset and traditional ground magnetic onset signatures. *J. Geophys. Res.: Space Phys.*, *118*(7), 4080–4092. https://doi.org/10.1002/jgra.50384

Lyons, L. R., Liu, J., Nishimura, Y., Reimer, A. S., Bristow, W. A., Hampton, D. L., Shi, X. L., Varney, R. H., and Donovan, E. F. (2021). Radar observations of flows leading to substorm onset over Alaska. *J. Geophys. Res.: Space Phys.*, *126*(2), e2020JA028147. https://doi.org/10.1029/2020JA028147

Matzka, J., Stolle, C., Yamazaki, Y., Bronkalla, O., and Morschhauser, A. (2021). The geomagnetic *Kp* index and derived indices of geomagnetic activity. *Space Wea.*, *19*(5), e2020SW002641. https://doi.org/10.1029/2020SW002641

McCrea, I., Aikio, A., Alfonsi, L., Belova, E., Buchert, S., Clilverd, M., Engler, N., Gustavsson, B., Heinselman, … Vierinen, J. (2015). The science case for the EISCAT_3D radar. *Prog. Earth Planet. Sci.*, *2*(1), 21. https://doi.org/10.1186/s40645-015-0051-8

McWilliams, K. A., Detwiller, M., Kotyk, K., Krieger, K., Rohel, R., Billett, D. D., Huyghebaert, D., and Ponomarenko, P. (2023). Borealis: an advanced digital hardware and software design for SuperDARN radar systems. *Radio Sci.*, *58*(3), e2022RS007591. https://doi.org/10.1029/2022RS007591

Mende, S. B., Harris, S. E., Frey, H. U., Angelopoulos, V., Russell, C. T., Donovan, E., Jackel, B., Greffen, M., and Peticolas, L. M. (2008). The THEMIS array of ground-based observatories for the study of auroral substorms. *Space Sci. Rev.*, *141*(1-4), 357–387. https://doi.org/10.1007/s11214-008-9380-x

Milan, S. E., Hubert, B., and Grocott, A. (2005). Formation and motion of a transpolar arc in response to dayside and nightside reconnection. *J. Geophys. Res.: Space Phys.*, *110*(A1), A01212. https://doi.org/10.1029/2004JA010835

Milan, S. E., Gosling, J. S., and Hubert, B. (2012). Relationship between interplanetary parameters and the magnetopause reconnection rate quantified from observations of the expanding polar cap. *J. Geophys. Res.: Space Phys.*, *117*(A3), A03226. https://doi.org/10.1029/2011JA017082

Milan, S. E., Imber, S. M., Lester, M., Nakamura, R., Boakes, P., Kauristie, K., Palmroth, M., Opgenoorth, H., and Sergeev, V. (2013). ECLAT: the European cluster assimilation technology project. In *Proceedings of the European Planetary Science Congress 2013* (pp. EPSC2013-1065). London: EPSC.

Milan, S. E., Imber, S. M., Carter, J. A., Walach, M. T., and Hubert, B. (2016). What controls the local time extent of flux transfer events?. *J. Geophys. Res.: Space Phys.*, *121*(2), 1391–1401. https://doi.org/10.1002/2015JA022012

Milan, S. E., Clausen, L. B. N., Coxon, J. C., Carter, J. A., Walach, M. T., Laundal, K., Østgaard, N., Tenfjord, P., Reistad, J., … Anderson, B. J. (2017). Overview of solar wind-magnetosphere-ionosphere-atmosphere coupling and the generation of magnetospheric currents. *Space Sci. Rev.*, *206*(1), 547–573. https://doi.org/10.1007/s11214-017-0333-0

Milan, S. E., Carter, J. A., Bower, G. E., Imber, S. M., Paxton, L. J., Anderson, B. J., Hairston, M. R., and Hubert, B. (2020). Dual-lobe reconnection and horse-collar auroras. *J. Geophys. Res.: Space Phys.*, *125*(10), e2020JA028567. https://doi.org/10.1029/2020JA028567

Moen, J., Oksavik, K., and Carlson, H. C. (2004). On the relationship between ion upflow events and cusp auroral transients. *Geophys. Res. Lett.*, *31*(11), L11808. https://doi.org/10.1029/2004GL020129

Nishimura, Y., Lyons, L. R., Nicolls, M. J., Hampton, D. L., Michell, R. G., Samara, M., Bristow, W. A., Donovan, E. F., Spanswick, E., … Mende, S. B. (2014). Coordinated ionospheric observations indicating coupling between preonset flow bursts and waves that lead to substorm onset. *J. Geophys. Res.: Space Phys.*, *119*(5), 3333–3344. https://doi.org/10.1002/2014JA019773

Nishimura, Y., Yang, J., Pritchett, P. L., Coroniti, F. V., Donovan, E. F., Lyons, L. R.,

Wolf, R. A., Angelopoulos, V., and Mende, S. B. (2016). Statistical properties of substorm auroral onset beads/rays. *J. Geophys. Res.: Space Phys.*, *121*(9), 8661–8676. https://doi.org/10.1002/2016JA022801

Ogawa, Y., Tanaka, Y., Kadokura, A., Hosokawa, K., Ebihara, Y., Motoba, T., Gustavsson, B., Brändström, U., Sato, Y., … Fujii, R. (2020). Development of low-cost multi-wavelength imager system for studies of aurora and airglow. *Polar Sci.*, *23*, 100501. https://doi.org/10.1016/j.polar.2019.100501

Oksavik, K., Moen, J., and Carlson, H. C. (2004). High-resolution observations of the small-scale flow pattern associated with a poleward moving auroral form in the cusp. *Geophys. Res. Lett.*, *31*(11), L11807. https://doi.org/10.1029/2004GL019838

Oksavik, K., Barth, V. L., Moen, J., and Lester, M. (2010). On the entry and transit of high-density plasma across the polar cap. *J. Geophys. Res.: Space Phys.*, *115*(A12), A12308. https://doi.org/10.1029/2010JA015817

Østgaard, N., Mende, S. B., Frey, H. U., Frank, L. A., and Sigwarth, J. B. (2003). Observations of non-conjugate theta aurora. *Geophys. Res. Lett.*, *30*(21), 2125. https://doi.org/10.1029/2003GL017914

Østgaard, N., Humberset, B. K., and Laundal, K. M. (2011a). Evolution of auroral asymmetries in the conjugate hemispheres during two substorms. *Geophys. Res. Lett.*, *38*(3), L03101. https://doi.org/10.1029/2010GL046057

Østgaard, N., Laundal, K. M., Juusola, L., Åsnes, A., Håland, S. E., and Weygand, J. M. (2011b). Interhemispherical asymmetry of substorm onset locations and the interplanetary magnetic field. *Geophys. Res. Lett.*, *38*(8), L08104. https://doi.org/10.1029/2011GL046767

Østgaard, N., Reistad, J. P., Tenfjord, P., Laundal, K. M., Snekvik, K., Milan, S., and Haaland, S. (2015). Mechanisms that produce auroral asymmetries in conjugate hemispheres. In Y. L. Zhang, et al. (Eds.), *Auroral Dynamics and Space Weather* (pp. 131-143). Washington: American Geophysical Union. https://doi.org/10.1002/9781118978719.ch10

Østgaard, N., Reistad, J. P., Tenfjord, P., Laundal, K. M., Rexer, T., Haaland, S. E., Snekvik, K., Hesse, M., Milan, S. E., and Ohma, A. (2018). The asymmetric geospace as displayed during the geomagnetic storm on August 17, 2001. In *Proceedings of the 20th EGU General Assembly* (pp. 2553). Vienna, Austria: EGU.

Paxton, L. J., and Anderson, D. E. (1992). Far ultraviolet remote sensing of venus and mars. In J. G. Luhmann, et al. (Eds.), *Venus and Mars: Atmospheres, Ionospheres, and Solar Wind Interactions* (pp. 113-189). Washington: American Geophysical Union. https://doi.org/10.1029/GM066p0113

Paxton, L. J., and Zhang, Y. (2016). *Far Ultraviolet Imaging of the Aurora in Space Weather Fundamentals*. CRC Press.

Pfaff, Jr. R. F. (2020). Using measurements on multiple satellites arranged in global, regional, and local configurations to obtain fundamental knowledge of the earth's upper atmosphere/ionosphere system - the great prospects of NASA's geospace dynamics constellation. In *Proceedings of the American Geophysical Union, Fall Meeting 2020* (pp. SA018-01). AGU.

Raab, W., Branduardi-Raymont, G., Wang, C., Dai, L., Donovan, E., Enno, G., Escoubet, P., Holland, A., Jing, L., … Zheng, J. H. (2016). SMILE: a joint ESA/CAS mission to investigate the interaction between the solar wind and Earth's magnetosphere. In *Proceedings of SPIE 9905, Space Telescopes and Instrumentation 2016: Ultraviolet to Gamma Ray* (pp. 1-9). Edinburgh: SPIE. https://doi.org/10.1117/12.2231984

Reidy, J. A., Fear, R. C., Whiter, D. K., Lanchester, B. S., Kavanagh, A. J., Paxton, L. J., Zhang, Y., and Lester, M. (2017). Multi-instrument observation of simultaneous polar cap auroras on open and closed magnetic field lines. *J. Geophys. Res.: Space Phys.*, *122*(4), 4367–4386. https://doi.org/10.1002/2016JA023718

Reistad, J. P., Østgaard, N., Tenfjord, P., Laundal, K. M., Snekvik, K., Haaland, S., Milan, S. E., Oksavik, K., Frey, H. U., and Grocott, A. (2016). Dynamic effects of restoring footpoint symmetry on closed magnetic field lines. *J. Geophys. Res.: Space Phys.*, *121*(5), 3963–3977. https://doi.org/10.1002/2015JA022058

Roelof, E. C., and Sibeck, D. G. (1993). Magnetopause shape as a bivariate function of interplanetary magnetic field *Bz* and solar wind dynamic pressure. *J. Geophys. Res.: Space Phys.*, *98*(A12), 21421–21450. https://doi.org/10.1029/93JA02362

Samsonov, A., Sembay, S., Read, A., Carter, J. A., Branduardi-Raymont, G., Sibeck, D., and Escoubet, P. (2022). Finding magnetopause standoff distance using a soft x-ray imager: 2. methods to analyze 2-D X-ray images. *J. Geophys. Res.: Space Phys.*, *127*(12), e2022JA030850. https://doi.org/10.1029/

2022JA030850

Sandholt, P. E., Farrugia, C. J., and Cowley, S. W. H. (1998). Pulsating cusp aurora for northward interplanetary magnetic field. *J. Geophys. Res.: Space Phys.*, 103(A11), 26507–26520. https://doi.org/10.1029/98JA02433

Shi, X., Hartinger, M. D., Baker, J. B. H., Ruohoniemi, J. M., Lin, D., Xu, Z., Coyle, S., Kunduri, B. S. R., Kilcommons, L. M., and Willer, A. (2020). Multipoint conjugate observations of dayside ULF waves during an extended period of radial IMF. *J. Geophys. Res.: Space Phys.*, 125(11), e2020JA028364. https://doi.org/10.1029/2020JA028364

Shiokawa, K., Katoh, Y., Hamaguchi, Y., Yamamoto, Y., Adachi, T., Ozaki, M., Oyama, S. I., Nosé, M., Nagatsuma, T., … Karjala, M. (2017). Ground-based instruments of the PWING project to investigate dynamics of the inner magnetosphere at subauroral latitudes as a part of the ERG-ground coordinated observation network. *Earth, Planets Space*, 69(1), 160. https://doi.org/10.1186/s40623-017-0745-9

Sibeck, D. G., Allen, R., Aryan, H., Bodewits, D., Brandt, P., Branduardi-Raymont, G., Brown, G., Carter, J. A., Collado-Vega, Y. M., … Wing, S. (2018). Imaging plasma density structures in the soft X-rays generated by solar wind charge exchange with neutrals. *Space Sci. Rev.*, 214(4), 79. https://doi.org/10.1007/s11214-018-0504-7

Smith, A. W., Rae, I. J., Forsyth, C., Watt, C. E. J., and Murphy, K. R. (2020). On the magnetospheric ULF wave counterpart of substorm onset. *J. Geophys. Res.: Space Phys.*, 125(4), e2019JA027573. https://doi.org/10.1029/2019JA027573

Smith, A. W., Rae, I. J., Forsyth, C., Watt, C. E. J., and Murphy, K. R. (2023). Statistical characterization of the dynamic near-earth plasma sheet relative to ultra-low frequency (ULF) wave growth at substorm onset. *J. Geophys. Res.: Space Phys.*, 128(1), e2022JA030491. https://doi.org/10.1029/2022JA030491

Spanswick, E., Donovan, E., Friedel, R., and Korth, A. (2007). Ground based identification of dispersionless electron injections. *Geophyis. Res. Lett.*, 34(3), L03101. https://doi.org/10.1029/2006GL028329

Tanaka, Y. M., Aso, T., Gustavsson, B., Tanabe, K., Ogawa, Y., Kadokura, A., Miyaoka, H., Sergienko, T., Brändström, U., and Sandahl, I. (2011). Feasibility study on generalized-aurora computed tomography. *Ann. Geophys.*, 29(3), 551–562. https://doi.org/10.5194/angeo-29-551-2011

Trattner, K. J., Fuselier, S. A., Petrinec, S. M., Yeoman, T. K., Mouikis, C., Kucharek, H., and Reme, H. (2005). Reconnection sites of spatial cusp structures. *J. Geophys. Res.: Space Phys.*, 110(A4), A04207. https://doi.org/10.1029/2004JA010722

Tsyganenko, N. A. (1995). Modeling the Earth's magnetospheric magnetic field confined within a realistic magnetopause. *J. Geophys. Res.: Space Phys.*, 100(A4), 5599–5612. https://doi.org/10.1029/94JA03193

Tsyganenko, N. A. (1996). Effects of the solar wind conditions in the global magnetospheric configurations as deduced from data-based field models (Invited). In *Proceedings of the 3rd International Conference Held in Versailles* (pp. 181). Paris: European Space Agency.

Tsyganenko, N. A. (2013). Data-based modelling of the Earth's dynamic magnetosphere: a review. *Ann. Geophys.*, 31(10), 1745–1772. https://doi.org/10.5194/angeo-31-1745-2013

Walach, M. T., and Grocott, A. (2019). SuperDARN observations during geomagnetic storms, geomagnetically active times, and enhanced solar wind driving. *J. Geophys. Res.: Space Phys.*, 124(7), 5828–5847. https://doi.org/10.1029/2019JA026816

Walach, M. T., Grocott, A., and Milan, S. E. (2021). Average ionospheric electric field morphologies during geomagnetic storm phases. *J. Geophys. Res.: Space Phys.*, 126(4), e2020JA028512. https://doi.org/10.1029/2020JA028512

Walach, M. T., Grocott, A., Thomas, E. G., and Staples, F. (2022). Dusk-dawn asymmetries in SuperDARN convection maps. *J. Geophys. Res.: Space Phys.*, 127(12), e2022JA030906. https://doi.org/10.1029/2022JA030906

Walsh, B., Sibeck, D., Cravens, T., Galeazzi, M., Collier, M., Porter, F., Sembay, S., Connor, H., Kuntz, K., … Nutter, R. (2021). Lunar Environment heliospheric X-ray Imager (LEXI). In *Proceedings of the 43rd COSPAR Scientific Assembly* (pp. 789).

Walsh, B. M., Foster, J. C., Erickson, P. J., and Sibeck, D. G. (2014a). Simultaneous ground- and space-based observations of the plasmaspheric plume and reconnection. *Science*, 343(6175), 1122–1125. https://doi.org/10.1126/science.1247212

Walsh, B. M., Phan, T. D., Sibeck, D. G., and Souza, V. M. (2014b). The plasmaspheric plume and magnetopause reconnection. *Geophys. Res. Lett.*, 41(2), 223–228. https://doi.org/10.1002/2013GL058802

Wang, C. (2010). New chains of space weather monitoring stations in China. *Space Wea.*, 8(8), S08001. https://doi.org/10.1029/2010SW000603

Wang, C., Chen, Z. Q., and Xu, J. Y. (2020). Introduction to Chinese meridian project-phase Ⅱ. *Chin. J. Space Sci.*, 40(5), 718–722. https://doi.org/10.11728/cjss2020.05.718

Wang, C., Xu, J. Y., Lü, D. R., Yue, X. N., Xue, X. H., Chen, G., Yan, J. Y., Yan, Y. H., Lan, A. L., … Tian, Y. F. (2022). Construction progress of Chinese meridian project phase Ⅱ. *Chin. J. Space Sci.*, 42(4), 539–545. https://doi.org/10.11728/cjss2022.04.yg09

Waters, C. L., Anderson, B. J., Green, D. L., Korth, H., Barnes, R. J., and Vanhamäki, H. (2020). Science data products for AMPERE. In M. W. Dunlop, ed. (Eds.), *Ionospheric Multi-Spacecraft Analysis Tools: Approaches for Deriving Ionospheric Parameters* (pp. 141-165). Cham: Springer. https://doi.org/10.1007/978-3-030-26732-2_7.

Wei, D., Dunlop, M. W., Yang, J. Y., Dong, X. C., Yu, Y. Q., and Wang, T. (2021). Intense dB/dt variations driven by near-earth bursty bulk flows (BBFs): a case study. *Geophys. Res. Lett.*, 48(4), e2020GL091781. https://doi.org/10.1029/2020GL091781

Wild, J. A., Cowley, S. W. H., Davies, J. A., Khan, H., Lester, M., Milan, S. E., Provan, G., Yeoman, T. K., Balogh, A., … Georgescu, E. (2001). First simultaneous observations of flux transfer events at the high-latitude magnetopause by the Cluster spacecraft and pulsed radar signatures in the conjugate ionosphere by the CUTLASS and EISCAT radars. *Ann. Geophys.*, 19(10-12), 1491–1508. https://doi.org/10.5194/angeo-19-1491-2001

Wild, J. A., Milan, S. E., Cowley, S. W. H., Dunlop, M. W., Owen, C. J., Bosqued, J. M., Taylor, M. G. G. T., Davies, J. A., Lester, M., … Rème, H. (2003). Coordinated interhemispheric SuperDARN radar observations of the ionospheric response to flux transfer events observed by the Cluster spacecraft at the high-latitude magnetopause. *Ann. Geophys.*, 21(8), 1807–1826. https://doi.org/10.5194/angeo-21-1807-2003

Wild, J. A., Milan, S. E., Owen, C. J., Bosqued, J. M., Lester, M., Wright, D. M., Frey, H., Carlson, C. W., Fazakerley, A. N., … Rème, H. (2004). The location of the open-closed magnetic field line boundary in the dawn sector auroral ionosphere. *Ann. Geophys.*, 22(10), 3625–3639. https://doi.org/10.5194/angeo-22-3625-2004

Wild, J. A., Milan, S. E., Davies, J. A., Dunlop, M. W., Wright, D. M., Carr, C. M., Balogh, A., Rème, H., Fazakerley, A. N., and Marchaudon, A. (2007). On the location of dayside magnetic reconnection during an interval of duskward oriented IMF. *Ann. Geophys.*, 25(1), 219–238. https://doi.org/10.5194/angeo-25-219-2007

Xu, Z., Hartinger, M. D., Clauer, C. R., Peek, T., and Behlke, R. (2017). A comparison of the ground magnetic responses during the 2013 and 2015 St. Patrick's Day geomagnetic storms. *J. Geophys. Res.: Space Phys.*, 122(4), 4023–4036. https://doi.org/10.1002/2016JA023338

Xu, Z., Hartinger, M. D., Oliveira, D. M., Coyle, S., Clauer, C. R., Weimer, D., and Edwards, T. R. (2020). Interhemispheric asymmetries in the ground magnetic response to interplanetary shocks: the role of shock impact angle. *Space Wea.*, 18(3), e2019SW002427. https://doi.org/10.1029/2019SW002427

Yamazaki, Y., Matzka, J., Stolle, C., Kervalishvili, G., Rauberg, J., Bronkalla, O., Morschhauser, A., Bruinsma, S., Shprits, Y. Y., and Jackson, D. R. (2022). Geomagnetic activity index hpo. *Geophys. Res. Lett.*, 49(10), e2022GL098860. https://doi.org/10.1029/2022GL098860

Yang, J. Y., Dunlop, M. W., Lühr, H., Xiong, C., Yang, Y. Y., Cao, J. B., Wild, J. A., Li, L. Y., Ma, Y. D., … Ritter, P. (2018). Statistical correlation analysis of field-aligned currents measured by swarm. *J. Geophys. Res.: Space Phys.*, 123(10), 8170–8184. https://doi.org/10.1029/2018JA025205

Yee, J. H., Gjerloev, J., Misra, S., Laundal, K., and Perez, R. (2022). Electrojet Zeeman Imaging Explorer (EZIE): a CubeSat mission to study the electro-jets. In *Proceedings of the 44th COSPAR Scientific Assembly* (pp. 754).

Zhang, Q. H., Zhang, Y. L., Wang, C., Lockwood, M., Yang, H. G., Tang, B. B., Xing, Z. Y., Oksavik, K., Lyons, L. R., … Xia, L. D. (2020). Multiple transpolar auroral arcs reveal insight about coupling processes in the earth's magnetotail. *Proc. Natl. Acad. Sci. USA*, 117(28), 16193–16198. https://doi.org/10.1073/pnas.2000614117